Modeling of ecosystem processes on the Oregon shelf during the 2001 summer upwelling

Y. H. Spitz and J. S. Allen

College of Oceanic and Atmospheric Sciences, Oregon State University, Corvallis, Oregon, USA

J. Gan

Department of Mathematics and Atmospheric, Marine and Coastal Environment Program, Hong Kong University of Science and Technology, Kowloon, Hong Kong

Received 7 January 2005; revised 16 June 2005; accepted 19 August 2005; published 22 October 2005.

[1] Three-dimensional ecosystem response to wind forcing on the continental shelf off Oregon is studied using a five-component nitrogen-based ecosystem model coupled to a high-resolution circulation model. We investigate, in particular, the influence of time-dependent winds and alongshore variations in shelf topography for summer 2001 during the time period of the Coastal Ocean Advances in Shelf Transport (COAST) field experiment. Over summer 2001 the average southward, upwelling-favorable wind leads to the development of a southward coastal jet and upwelled cold nutrient-rich water over the shelf. A strong influence of the shelf topography is found in the observed and modeled nutrients and plankton, with significant spatial variability associated with interactions of the shelf flow with Heceta Bank. The model results show that the largest mean chlorophyll-a concentrations are located onshore of the coastal jet, while the largest mean zooplankton concentrations are found farther offshore, typically on the offshore side of the jet, except on Heceta Bank. During intermittent downwelling periods the largest concentrations of mean zooplankton and phytoplankton, however, are both inshore of the jet. The 20 day oscillations in the modeled nutrients and plankton, the time lags between the wind stress and these ecosystem components, and the decorrelation timescales of phytoplankton agree with those obtained from mooring and satellite measurements. A detailed analysis of the balance between biological and physical forcing helps to clarify the temporal and spatial response of the ecosystem.

Citation: Spitz, Y. H., J. S. Allen, and J. Gan (2005), Modeling of ecosystem processes on the Oregon shelf during the 2001 summer upwelling, *J. Geophys. Res.*, *110*, C10S17, doi:10.1029/2005JC002870.

1. Introduction

[2] The Oregon coast has long been recognized as a region of strong summer upwelling in direct response to prevailing southward winds. Field experiments starting with those in 1972 and 1973 as part of the Coastal Upwelling Ecosystem Analysis (CUEA) program and recently in 2001 as part of the Coastal Ocean Advances in Shelf Transport (COAST) program [*Smith*, 1974; *Huyer*, 1983; *Barth et al.*, 2000; *Austin and Barth*, 2002; *Castelao and Barth*, 2005; *Kosro*, 2005] and modeling studies [*Oke et al.*, 2002; *Gan et al.*, 2005; *Gan and Allen*, 2005] show that circulation patterns over the continental shelf are quite different immediately north and south of Newport (44.6°N). North of Newport, where the coastline is relatively straight and the shelf narrow, a southward coastal jet is found close to shore and the across-shelf circulation shows some similarities with that in two-dimensional conceptual models. South of Newport and especially over Heceta Bank, complex flow patterns are associated with the irregularities in the shelf topography. In this region, the coastal jet is displaced offshore and a cyclonic recirculation exists inshore of the jet during periods of southward wind relaxation.

[3] During upwelling, cold nutrient-rich water is drawn up to the surface, leading to high productivity and standing stock in a region close to shore [*Small and Menzies*, 1981; *Karp-Boss et al.*, 2004]. Analysis of surface chlorophyll-*a* fields from Sea-viewing Wide Field of view Sensor (SeaWiFS) images during the years 1999–2001 [*Bosch et al.*, 2002] has shown complex spatial patterns along the Oregon coast. Enhancement and offshore extension of the chlorophyll-*a* concentrations were observed over Heceta Bank compared to the other regions along the coast. In addition, the magnitude of the upwelling summer bloom displayed some interannual variability. Surface chlorophyll-*a* concentrations were the highest during summer 2001. During the COAST study [*Lamb and Peterson*, 2005], zooplankton were sampled in a region from 44°N to 45°N. It was found that the biomass of copepods was very low at stations beyond the shelf break (200 m water

0148-0227/05/2005JC002870$09.00

Table 1. Model Parameters

Parameter	Symbol	Value
Light attenuation due to sea water, m^{-1}	k_w	0.067
Light attenuation by phytoplankton, 10^{-3} m^2 (mmol N)$^{-1}$	k_p	9.5
Initial slope of *P-I* curve, d^{-1} (W m^{-2})$^{-1}$	α	0.025
Phytoplankton maximum uptake rate, d^{-1}	V_m	1.5
Half-saturation for phytoplankton NO_3 uptake, mmol N m^{-3}	K_u	1.0
Half-saturation for phytoplankton NH_4 uptake, mmol N m^{-3}	K_u	1.0
NH_4 inhibition parameter, (mmol N m^{-3})$^{-1}$	Ψ	1.46
NH_4 oxidation coefficient, d^{-1}	Ω	0.25
Detritus decomposition rate, d^{-1}	Φ	0.1
Phytoplankton specific mortality rate, d^{-1}	Ξ	0.1
Zooplankton specific excretion, mortality rate, d^{-1}	Γ	0.3
Zooplankton maximum grazing rate, d^{-1}	R_m	0.6
Ivlev constant, mmol N m^{-3}	λ	0.15
Fraction of zooplankton grazing egested, %	g	30
Detritus sinking rate, m d^{-1}	w_d	8.0

depth) while larger concentrations were found over the shelf, suggesting retention of zooplankton on the shelf and little net loss of zooplankton to offshore water by across-shore advection.

[4] Modeling of the Oregon coast ecosystem response to upwelling has previously been studied in a two-dimensional framework [*Wroblewski*, 1977; *Edwards et al.*, 2000; *Spitz et al.*, 2003; *Newberger et al.*, 2003]. Simulations with wind forcing from summer 1973 and 1999 [*Spitz et al.*, 2003] lead to a mean phytoplankton concentration maximum in the surface layer onshore of the upwelling jet and a mean zooplankton concentration maximum farther offshore. The locations and magnitudes of the maxima depend upon the nature of the time variability of the wind forcing and on the biological parameters (e.g., zooplankton grazing rate). Based upon field observations, the interaction of the wind-forced flow with spatially variable coastal topography can lead to a complex time- and space-dependent three-dimensional response of the ecosystem to upwelling, which requires application of a three-dimensional coupled circulation/ecosystem model for direct simulation.

[5] In the present study, we apply a three-dimensional coupled circulation/ecosystem numerical model to elucidate the physical and biological mechanisms involved in determining the alongshelf and across-shelf distribution of biomass during summer 2001, when the Coastal Ocean Advances in Shelf Transport (COAST) experiment took place. The model is a five-component nitrogen-based model since silicate and iron have not been found to be limiting nutrients along the Oregon coast during summer upwelling [*Corwith and Wheeler*, 2002; *Chase et al.*, 2005].

[6] The ecosystem model and its coupling to the circulation model are described in section 2. An initial qualitative assessment of the applicability of the ecosystem model is presented in section 3 through a comparison of the modeled surface chlorophyll-*a* with SeaWiFS observations for one 8 day period of sustained upwelling-favorable wind and another 8 day period of wind relaxation. Basic descriptions of the time average and the temporal evolution of the ecosystem variables are presented in section 4. The ecosystem response during two 10 day periods of different wind conditions, including an analysis of the balance between the physical and biological forcing mechanisms, is described in section 5. A summary is presented in section 6.

2. Coupled Circulation/Ecosystem Model

[7] A five-component nitrogen-based ecosystem model [*Spitz et al.*, 2003], including nitrate (NO_3), ammonium (NH_4), phytoplankton (P), zooplankton (Z) and detritus (D), is coupled to the Princeton Ocean Model (POM) [*Blumberg and Mellor*, 1987] and applied to the Oregon coast during summer 2001 [*Gan and Allen*, 2005]. The ecosystem model equations are given by

$$\frac{\partial \mathrm{NO_3}}{\partial t} = \Omega \mathrm{NH_4} - V_m f(I)\left\{\frac{\mathrm{NO_3}}{K_u + \mathrm{NO_3}} e^{-\psi \mathrm{NH_4}}\right\} P, \tag{1}$$

$$\frac{\partial \mathrm{NH_4}}{\partial t} = \phi D + \Gamma Z - V_m f(I)\left\{\frac{\mathrm{NH_4}}{K_u + \mathrm{NH_4}}\right\} P - \Omega \mathrm{NH_4}, \tag{2}$$

$$\frac{\partial P}{\partial t} = V_m f(I)\left\{\frac{\mathrm{NO_3}}{K_u + \mathrm{NO_3}} e^{-\psi \mathrm{NH_4}} + \frac{\mathrm{NH_4}}{K_u + \mathrm{NH_4}}\right\} P - R_m\left\{1 - e^{-\lambda P}\right\} Z - \Xi P, \tag{3}$$

$$\frac{\partial Z}{\partial t} = R_m(1-\gamma)\left\{1 - e^{-\lambda P}\right\} Z - \Gamma Z, \tag{4}$$

$$\frac{\partial D}{\partial t} = R_m \gamma\left\{1 - e^{-\lambda P}\right\} Z - \phi D - \Xi P - w_d \frac{\partial D}{\partial z}, \tag{5}$$

where t denotes time and z the vertical coordinate. The light limitation $f(I)$ is defined as

$$f(I) = \frac{aI}{\sqrt{V_m^2 + \alpha^2 I^2}}, \tag{6}$$

with $I(z, t) = I_0 \exp\left(k_w z + k_p \int_0^z P(z')dz'\right)$ and $-H_0 \le z \le 0$, so that the (positive) depth is $-z$.

[8] The effects of advection and diffusion are appropriately added to (1)–(5) when coupled to the POM physical circulation model. The parameters for the ecosystem model

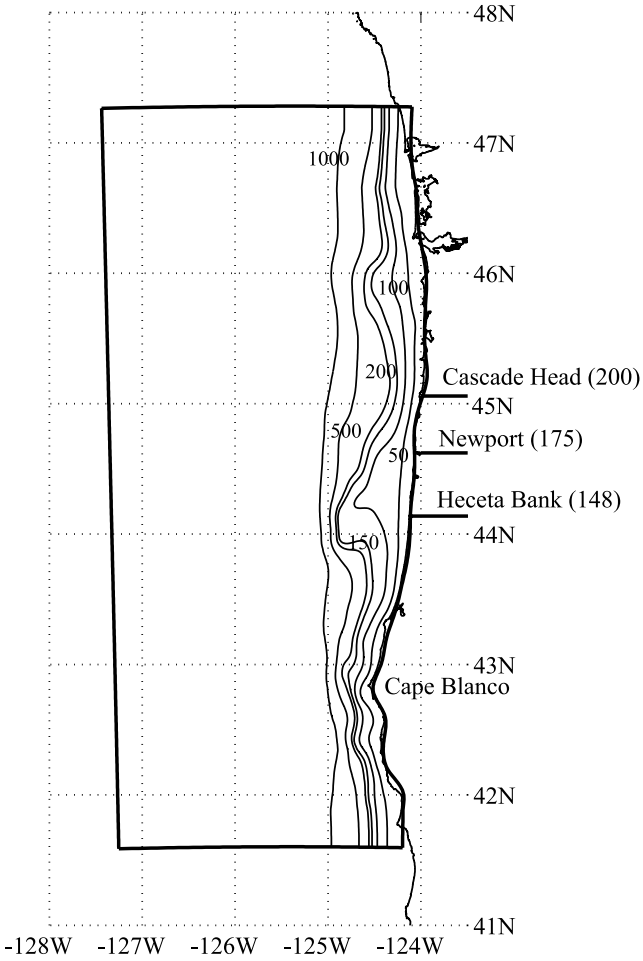

Figure 1. Model bathymetry with the 50, 100, 150, 200, 500, and 1000 m isobaths shown. The model domain (solid line) extends about 634 km alongshore and 250 km across-shore and contains three open boundaries. The locations of across-shore sections are labeled with their grid numbers and names.

differ somewhat from those used by *Spitz et al.* [2003] and are defined in Table 1. The zooplankton parameters are modified to represent better the dominant copepod species off the Oregon coast (*Acartia longiremis, Pseudocalanus mimus* and *Centropages abdominalis*) (W. Peterson, personal communication, 2003) and the detrital remineralization rate is reduced to 10% per day based upon observations of DON and PON during the COAST experiment [*Karp-Boss et al.*, 2004; P. A. Wheeler, personal communication, 2003]. Modeled chlorophyll-*a* is computed from modeled phytoplankton using a Chl:N ratio that varies from 2.0 mg Chl mmol N^{-1} near the coast to 0.6 mg Chl mmol N^{-1} offshore of the 200 m isobath. We base this conversion on the following observations. From a station 8 km offshore of Newport from July 1990 to August 1991, *Dickson* [1994] and *Dickson and Wheeler* [1995] obtained a Chl:N ratio of 2.19 ± 0.45 mg Chl mmol N^{-1}. At stations from 124°W to 126°W and from 44°N to 47°N during July 1985, *Kokkinakis and Wheeler* [1988] reported ratios varying from 1.8 mg Chl mmol N^{-1} onshore to as low as 0.3 mg Chl mmol N^{-1} offshore.

[9] The model domain is the same as that utilized by *Gan and Allen* [2005]. It extends alongshore 634 km from 41.7°N to about 47.3°N and offshore 250 km, with the coastline boundary fitted by a curvilinear coordinate system (Figure 1). The horizontal grid spacing is variable, with across-shore grid spacing of 1.5 km near the coast increasing to about 6 km in the western part of the domain and with alongshore spacing of 1 to 2 km. The model domain includes three open boundaries located on the north, south and west of the domain and is periodic in the alongshore direction. The details of the open offshore boundary condition specification are given by *Gan and Allen* [2005]. Realistic continental shelf and bottom topography off Oregon is utilized. The minimum depth is equal to 10 m and the maximum offshore depth is 1200 m. The vertical spacing is variable with 45 sigma levels and higher resolution near the surface and bottom.

[10] The atmospheric forcing is uniform in space, but varies in time. The wind stress (Figure 2) is calculated using the *Large and Pond* [1981] formulation and wind measurements from the NDBC mooring (44.62°N, 124.53°W, 130 m water depth) from 1 to 16 May 2001 and subsequently from the COAST meteorological buoy (44.99°N, 124.12°W, 80 m water depth). The surface heat flux is obtained from monthly mean climatological observations from 1 to 16 May 2001 and then from meteorological observations at the COAST meteorological buoy using bulk aerodynamic formulae as described by *Gan and Allen* [2002]. A 36 hour low-pass filter is applied to both the wind stress and the heat flux. Direct comparisons

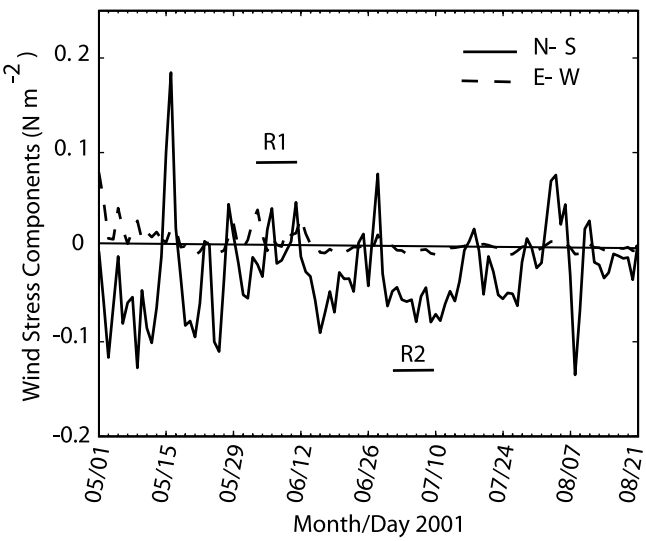

Figure 2. Wind stress components (N m^{-2}) from 1–16 May 2001 at the NDBC buoy (44.62°N, 124.53°W) and from 17 May to 21 August 2001 at the COAST meteorological buoy (44.99°N, 124.12°W). The solid line corresponds to the north-south component, and the dashed line corresponds to the east-west component. Two periods dominated by downwelling-favorable wind (R1, 3–12 June) and upwelling-favorable wind (R2, 1–10 July) are indicated. The mean values of the (alongshore (north-south), across-shore (east-west)) wind stress components (N m^{-2}) are (−0.028, 0.004) with standard deviations of (0.048, 0.012).

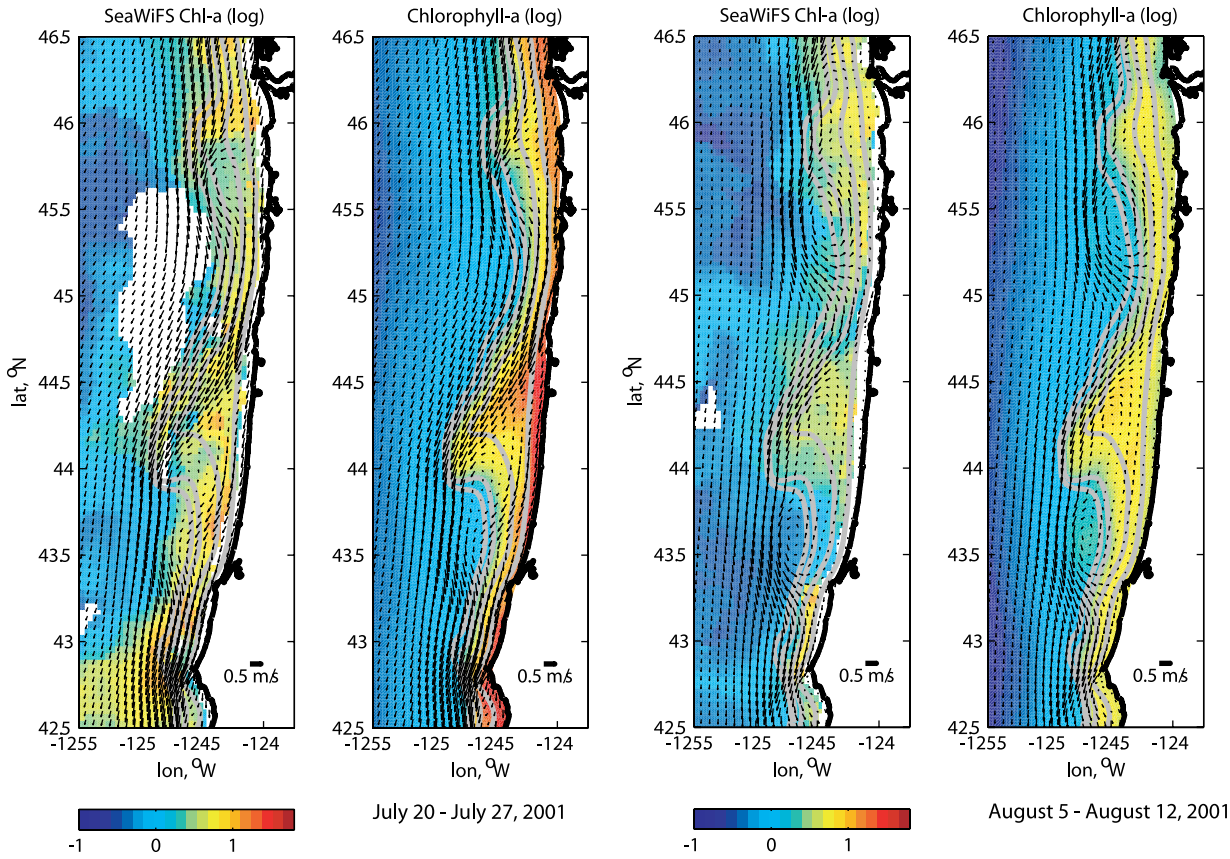

Figure 3. SeaWiFS and modeled surface chlorophyll-*a* (mg Chl m^{-3}) (left) during a period of sustained upwelling wind and (right) during a period following downwelling wind. The arrows represent the mean surface velocity vectors over the two chosen periods. Note that there are almost no SeaWiFS observations onshore of the 50 m isobath.

of measured currents and hydrographic fields with corresponding model variables of *Gan and Allen* [2005] show that the physical circulation model, set up and forced in this manner, does a reasonably good job of reproducing the observed shelf flow field. In addition, this model configuration isolates and allows study of alongshore variability induced solely by shelf bottom topography, which is an important objective of the COAST analysis efforts.

[11] The ecosystem initial conditions are horizontally uniform with profiles for nitrate and phytoplankton obtained from the observations offshore at 45°N on 18 May 2001, the first day of the COAST summer cruise in 2001 on the R/V *Thompson*. The initial profiles for the remaining variables are taken from a 1 year, one-dimensional run with small background diffusivity and without sinking [*Newberger et al.*, 2003]. Note that results of sensitivity tests show that the specification of the initial depth distribution of total nitrogen is an important factor in the subsequent ecosystem evolution. Here the initial depth profiles of nitrate and of phytoplankton, which constitute the largest fraction of the total nitrogen, are taken from measurements. The surface photosynthetically available radiation I_o is obtained from monthly mean climatological observations from 1 to 16 May 2001 and then from 36 hour low-pass-filtered solar radiation observations at the COAST meteorological buoy.

[12] The circulation model is started with zero velocities and horizontally uniform temperature and salinity profiles from climatological May values at a station 25 nautical miles off Newport (44.6°N). The coupled circulation/ecosystem model is started on 1 May 2001 and forced for 119 days. The first 22 days of the model simulation are regarded as spin-up period.

3. Observed and Modeled Surface Chlorophyll-*a*

[13] Sea surface chlorophyll-*a* from 8 day composite SeaWiFS images can be compared with corresponding model results to provide a useful qualitative assessment of the coupled physical/ecosystem model to represent the patterns and magnitudes of the surface chlorophyll-*a* fields (Figure 3). We chose two composite images that have particularly low cloud coverage. The observed chlorophyll-*a* fields show substantial variations in magnitude and spatial distribution between a period of sustained upwelling-favorable winds (20–27 July), characterized by relatively large concentrations, and a period following a downwelling wind event (5–12 August), with generally lower values. The model surface chlorophyll-*a* generally show qualitatively similar temporal and spatial variations. During the upwelling-favorable period (20–27 July), the highest levels of modeled chlorophyll-*a* are found inshore of the 50 m isobath, except in the vicinity of Heceta Bank (44.2°N–

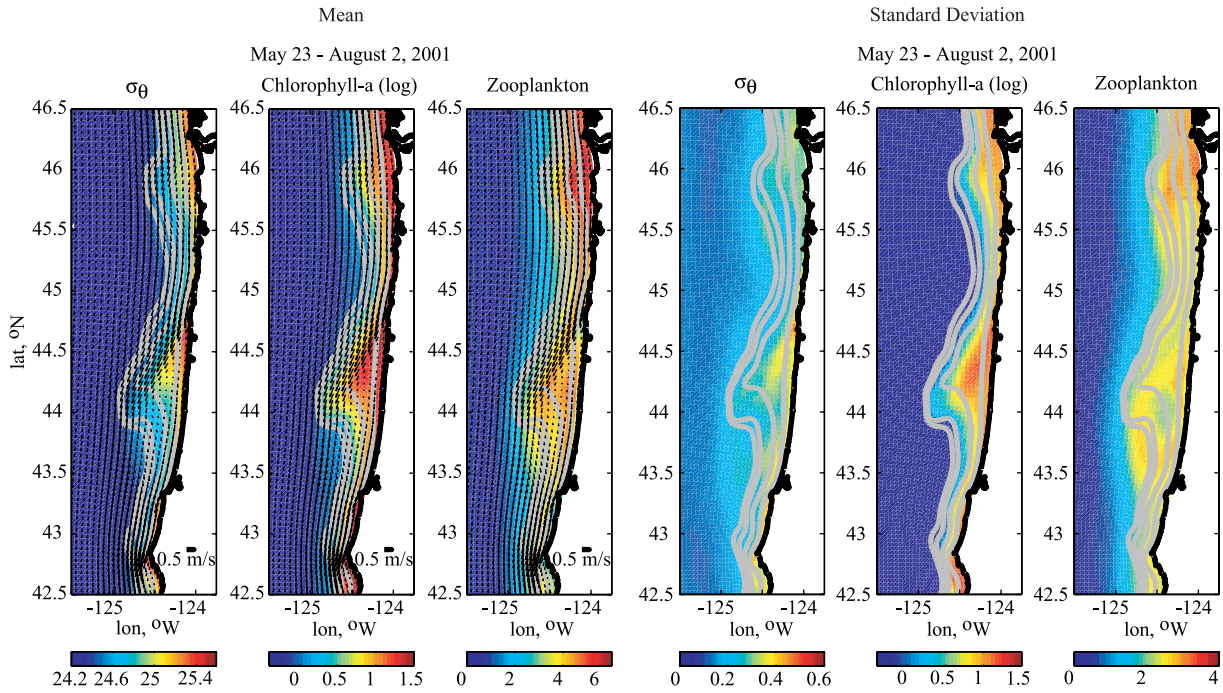

Figure 4. Mean and standard deviation of surface potential density σ_θ (kg m^{-3}), chlorophyll-*a* (mg Chl m^{-3}), and zooplankton (mmol N m^{-3}) between 23 May and 2 August 2001. The chlorophyll-*a* is plotted on a logarithmic (log 10) scale. The shaded lines are the 50, 100, 150, and 200 m isobaths. The arrows represent the mean surface velocity vectors.

44.6°N) where a tongue of higher chlorophyll-*a* extends offshore to the 100 m isobath. Note that there are almost no SeaWiFS observations inshore of the 50 m isobath, but similar chlorophyll-*a* patches are observed on Heceta Bank as well as around 46°N, where the shelf is wider. Following a downwelling-favorable wind period (5–12 August), a decrease of surface chlorophyll-*a* is observed nearshore, but elevated chlorophyll-*a* is still present in regions over the wider shelf. Thus the general temporal variability between different periods, the spatial patterns, and magnitudes of the observed and modeled chlorophyll-*a* fields are generally in reasonable agreement. Some discrepancies can be noted, however. For example, during upwelling, high chlorophyll-*a* around Cape Blanco is observed farther offshore than in the model simulation. After relaxation, the SeaWiFS image does not show the patch of high chlorophyll-*a* south of Heceta Bank that is present in the modeled field and can be associated there with the presence of an eddy. Three possible reasons for the discrepancy can be pointed out. First, a comparison of the physical circulation model variables with COAST observations of *Gan and Allen* [2005] shows that the model has difficulties in representing the complex spatially and temporally variable flow over the southern part of Heceta Bank in a deterministic manner. Thus eddy-like features, not exactly coincident with the observed fields, may occur occasionally in the model in that location. Second, our model is driven by a temporally variable but spatially uniform wind, which could explain the discrepancy found south of Heceta Bank where observed winds are typically stronger than in the model run [*Samelson et al.*, 2002; *Bane et al.*, 2005; *Gan et al.*, 2005]. Third, the modeled chlorophyll-*a* is an average over the period of 8 days while the SeaWiFS observations are composite images and include periods of cloud coverage when observations are not available.

4. Model Results for Summer 2001

[14] Simulation of the ecosystem response to upwelling off the Oregon coast during summer 2001 shows features that indicate strong effects of the bottom topography in addition to wind response. On average over the summer 2001, the winds are southward and upwelling-favorable (Figure 2), which leads to the development of a mean southward coastal jet and upwelled cold and nutrient rich water over the shelf. This flow, however, is strongly altered by the topography of Heceta Bank, 44°N (Figure 4). A full analysis and discussion of the effect of Heceta Bank on the upwelling circulation can be found in the work of *Gan and Allen* [2005].

4.1. Time Mean Fields

[15] Time mean surface chlorophyll-*a* and zooplankton from 23 May through 2 August (Figure 4) show the response of the ecosystem to the dominant southward upwelling-favorable winds as well as to the topographical changes along the Oregon coast. Relatively high mean values of chlorophyll-*a* and zooplankton are found on the shelf. The alongshore pattern and across-shore extension of these fields are strongly influenced by the topography. The upwelling jet mainly follows the coastline, except over Heceta Bank and around 46°N where it shifts offshore due to the broadening of the shelf in these regions. Likewise, the across-shore extension of high mean biomass is limited to the 50 m isobath in regions of narrow shelf where the core of the coastal jet is located within 10 km of the

coast. In regions of wider shelf where the coastal jet veers offshore, high biomass extends roughly to the 100 m isobath. High mean chlorophyll-*a* is typically associated with water with potential density greater than 25 kg m^{-3} and temperature less than 12°C. Along the entire coast of Oregon, the relatively large mean values of chlorophyll-*a* are located onshore of the coastal jet. Surface mean zooplankton show different alongshore distributions from surface mean phytoplankton, reflecting the fact that their response to upwelling is on different time- and space scales than the response of the phytoplankton. In the across-shore direction, the maximum mean zooplankton is located offshore of the maximum mean phytoplankton. The surface zooplankton shows highest mean around 46°N where the shelf is wider and the upwelling jet turns slightly offshore. Very low zooplankton is found in two regions near the coast, i.e., near 44.7°N and south of 43.5°N. These regions correspond to strong upwelling (potential density higher than 25.6 kg m^{-3}) and large variability (standard deviation of potential density exceeding 0.5 kg m^{-3}). A major qualitative difference in the surface spatial distributions of the density, the phytoplankton, and the zooplankton is visible in the standard deviation fields where the largest standard deviation in chlorophyll-*a* is found on Heceta Bank south of the maximum standard deviation in the surface potential density and north of the maximum standard deviation in zooplankton. A similar relative distribution of the standard deviations for zooplankton and phytoplankton is found around 46°N. The similarity of the spatial distribution of phytoplankton and zooplankton near 46°N and on Heceta Bank further illustrates the strong response of the ecosystem to the topography.

[16] The time mean across-shore sections of phytoplankton displayed in Figure 5 indicate that phytoplankton are found in the upper 50 m of the water column and the maximum concentration is onshore of the jet regardless the width of the shelf. The modeled phytoplankton distribution is in good agreement with COAST chlorophyll-*a* observations from bottle (P. A. Wheeler, personal communication, 2003) and from SeaSoar vertical profiles (e.g., vertical sections BB1–5 [*O'Malley et al.*, 2002; *Barth et al.*, 2003]). Consistent with the measurements, the modeled chlorophyll-*a* concentration is the highest in the upper 10 m of the water column and within 10 to 15 km offshore. At Cascade Head and Newport where the shelf is quite narrow and the coastal jet is close to shore, chlorophyll-*a* decreases to a small value within 20 km offshore and a deep maximum is found at around 30 m depth. As the shelf widens, the region of high chlorophyll-*a* extends farther offshore. At Heceta Bank, chlorophyll-*a* remains quite high in the upper 10 m to about 40 km offshore before decreasing. From 40 km to about 100 km offshore, a deep chlorophyll-*a* maximum is found between 30 and 50 m depth and it deepens offshore although the concentrations are relatively small. The maximum of chlorophyll-*a* on the bank is located in a region next to the coast, which contains a mean weak southward flow that is separated from the main coastal jet.

[17] In contrast to the mean phytoplankton, the high value of mean zooplankton can be located either onshore or offshore of the upwelling jet depending on the width of the shelf (Figure 5). At Cascade Head and Newport, the shelf and the jet are relatively narrow and the local across-shore maximum of zooplankton is found offshore of the jet. South of Newport (e.g., at Heceta Bank), the shelf widens and the jet veers offshore. The local maximum of mean zooplankton is found onshore of the jet with high zooplankton spanning from the coast to the jet center. Close to shore (within 10 km offshore), there is a region with a very low concentration of zooplankton. This is due to upwelling there of water that is low in zooplankton biomass (see term balance discussion in section 5.2). At all of the sections displayed in Figure 5, the local maximum in mean zooplankton is offshore of the local maximum of mean phytoplankton. In addition, the across-shore scale of the region of relatively high mean zooplankton is larger than that of high phytoplankton. In our simulation, the zooplankton biomass is concentrated in the upper 50 m with a maximum in the upper 20 m. This is consistent with the MOCNESS observations in August 2001 [*Lamb and Peterson*, 2005] showing that the maximum mean biomass for three of the four dominant copepod species (*Acartia longiremis, Pseudocalanus mimus* and *Centropages abdominalis*) are found from the surface to 20 m and more than 80% of the biomass is concentrated in the upper 50 m.

[18] The sections of mean nitrate display similar patterns to that of mean density with an upward tilt toward the coast of the isoclines. However, differences are present near the coast. While the 25.5 kg m^{-3} isopycnal reaches the surface, the corresponding 20.3 mmol N m^{-3} isocline does not. This is a result of high biological activity, which leads to depletion of nitrate near the surface on the inner shelf. Another feature of interest is the pool of high-nitrate water on the bottom of the shelf at Heceta Bank where high-density water ($\sigma_\theta \approx 26.6$ kg m^{-3}) is also found. This high-nutrient, high-density water is disconnected in this section from the water farther offshore with the same high values of nutrient and density and is a result of three-dimensional advective flow processes induced by the bank topography [*Gan and Allen*, 2005]. The pool of high nutrient on the bottom of the shelf is not consumed by the phytoplankton due to the lack of light at that depth.

[19] Detritus is found over the shelf with higher concentrations from 10 m to about 80 m deep and with a maximum around 30 m. Values of modeled detritus below 85 m at Cascade Head are of the same order of magnitude as those found from particulate organic nitrogen (PON) measurements [*Karp-Boss et al.*, 2004], which are mainly measurements of nonliving material at that depth. Owing to a high remineralization rate of the pool of detritus, ammonium concentration is elevated in the same depth range as the detritus concentration. The maximum mean ammonium concentration is found at a depth of about 20 m, which is also consistent with measurements during summer 2001 (P. A. Wheeler, personal communication, 2003). Near the coast to about 10 km offshore, surface ammonium is depleted due to an uptake by phytoplankton, while some small concentrations of detritus are still present in the surface layer.

4.2. Temporal Evolution of Various Fields

[20] The time evolution of surface nitrate, phytoplankton and zooplankton at three locations along the Oregon coast

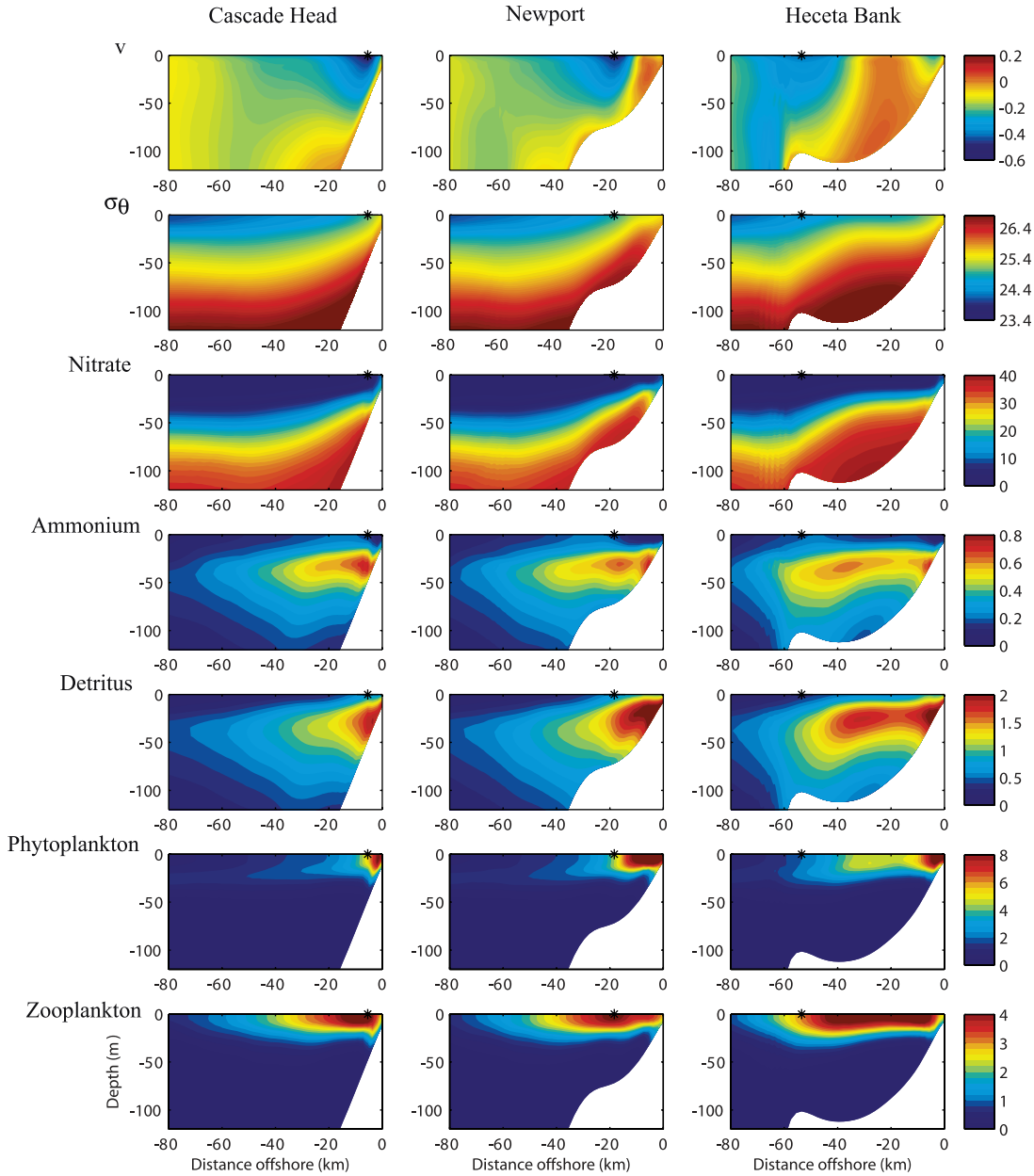

Figure 5. Time mean of the alongshore velocity v (m s^{-1}), the potential density σ_θ (kg m^{-3}), and the five components of the ecosystem model (mmol N m^{-3}) from 23 May through 2 August 2001 at three sections (Cascade Head (200), Newport (175), and Heceta Bank (148)). The star corresponds to the position of the core of the coastal jet, defined as the location of the maximum southward alongshore velocity v at the surface.

(Figure 6) clearly indicates the combined response of the ecosystem to upwelling and downwelling events as well as to topographical features such as the shelf width. First, note that the spin-up of the coupled ecosystem and circulation models takes about 20 days, which is clearly shown by the very low surface zooplankton until 22 May. While high surface nitrate concentrations are limited to a narrow region close to the coast at all three sections, the shelf width strongly influences the offshore extent of high phytoplankton and zooplankton concentrations, especially during the month of July when the alongshore wind is mostly southward and upwelling-favorable. During that month, high phytoplankton concentrations extend offshore about 10 km at Cascade Head, 25 km at Newport and 40 km over Heceta Bank. High zooplankton concentrations also extend farther offshore as the shelf widens. These are found offshore of the high phytoplankton concentrations and also offshore of the coastal jet, except over Heceta Bank where the coastal jet is much farther offshore than at the two other locations. Periods of upwelling, downwelling and relaxation are in general characterized by the same response of the various ecosystem components at the three sections. High nitrate and phytoplankton, and low zooplankton concentrations within 10 km from the coast are characteristic of the

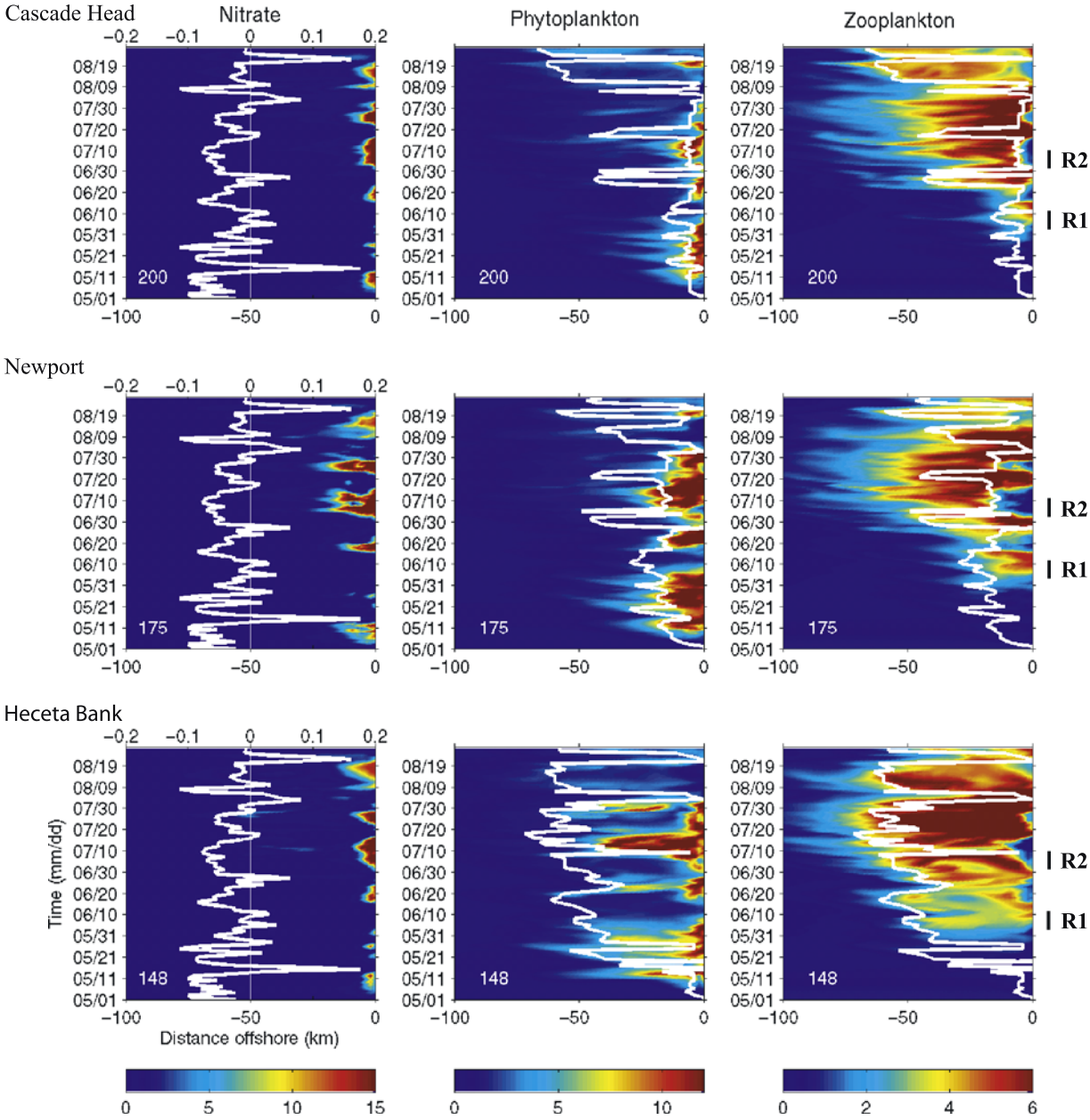

Figure 6. Time evolution of surface nitrate (mmol N m^{-3}), phytoplankton (mmol N m^{-3}), and zooplankton (mmol N m^{-3}) at three sections (Cascade Head (200), Newport (175), and Heceta Bank (148)). The white line in the left panel represents the north-south component of the wind stress (N m^{-2}). The white line in the middle and right panels represents the position of the core of the coastal jet.

upwelling events (e.g., 9–18 June, 1–10 July). Lower nitrate and chlorophyll-*a*, and higher zooplankton concentrations near the coast are found during periods of relaxation and downwelling (e.g., 22–30 June), even though the center of the coastal jet is farther offshore than during upwelling. During periods of alternate upwelling and downwelling (e.g., 13 May–12 June), there is no nitrate increase at the surface but the phytoplankton biomass increases as the grazers grow more slowly and do not control the growth of phytoplankton. On several occasions (e.g., 20–30 June, 27–31 July), phytoplankton on Heceta Bank display two maxima that are separated by lower values. This spatial pattern is also observed in the chlorophyll-*a* field during COAST sampling [*Barth et al.*, 2003, 2005]. From Figure 6, we can see a time lag between the changes in the wind and the response in the surface nitrate with additional time lags for the response of the phytoplankton and zooplankton. This can be further seen in the time series in Figure 7 where nitrate, phytoplankton and zooplankton concentrations have been spatially averaged over the shelf.

[21] The temporal variations in the spatially averaged nitrate, phytoplankton and zooplankton concentrations over the shelf and to 60 m deep (Figure 7) display strong oscillations with roughly 20 day period. Similar oscillations

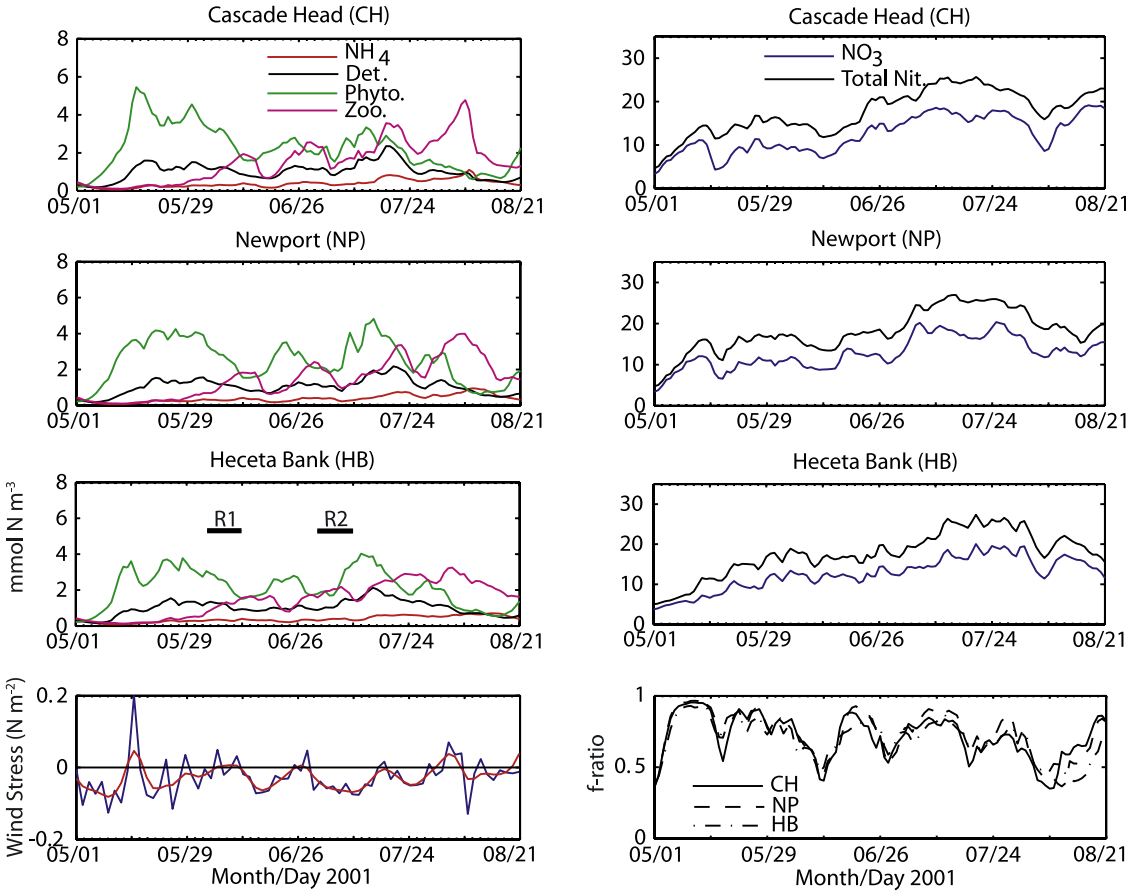

Figure 7. Time evolution of the spatially averaged concentrations and *f* ratio at three sections. The spatial average is across-shore and with depth. It extends over the upper ocean coastal (UOC) region, i.e., from the surface to 60 m depth (or the bottom) and from the coast to the 200 m isobath. The blue line in the lower left panel corresponds to the north-south component of the wind stress used to force the circulation model. The red line of the lower left panel is the 8 day low-pass-filtered north-south wind stress component.

have been noted by *Bane et al.* [2005] in their analysis of the alongshore wind stress and of the sea surface temperature from the six moorings deployed during COAST. While shorter timescale fluctuations exist in the fluorescence measurements at the mooring deployed since 2000 near Newport (44.65°N, 124.3°W), the 8 day low-pass-filtered observations also show strong oscillations at 20 day period (R. Letelier, unpublished data, 2003). From the calculation of the lagged correlation between the wind stress and the model variables, the temperature and nitrate are estimated to lag the wind stress by 3 to 4 days, which is similar to the lag observed in the temperature from the moorings [*Bane et al.*, 2005]. The phytoplankton lag wind stress by about 7 days and lag nitrate by roughly 3 to 4 days. Similar lags between phytoplankton and wind stress (6–10 days) have been observed in upwelling regions along the California coast [*Dugdale and Wilkerson*, 1989; *Service et al.*, 1998]. The zooplankton display a longer lag with the wind stress of roughly 13 days at Cascade Head (CH) to roughly 16 days at Heceta Bank (HB). Characteristics of the fluctuations in phytoplankton are similar at Newport (NP) and Heceta Bank (HB). In contrast, fluctuations in zooplankton are notably weaker at HB than at NP or CH. Decorrelation timescales (computed as the time lag for the autocorrelation to reach a value of 0.1) over the shelf at the three sections are approximately 6 to 8 days for the phytoplankton. These values are comparable to the decorrelation timescales of 10 days found from the analysis of satellite images of chlorophyll-*a* fields offshore in the California Current over larger spatial scale with wavelengths 50–150 km [*Denman and Abbott*, 1988, 1994] and from modeling of the ecosystem response to wind forcing over similar large spatial scales during summer 2000 [*Powell et al.*, 2005].

5. Ecosystem Response During Times of Different Wind Conditions

[22] *Gan and Allen* [2005] show that the strength and location of the coastal jet depend strongly upon the wind conditions. During a period of weak fluctuating northward wind (e.g., 3–12 June, R1), the coastal jet is weaker and farther offshore on the bank than during a period of sustained southward wind (e.g., 1–10 July, R2). In addition, during R1, northward currents are present inshore of the jet and contribute to a cyclonic circulation over and south of

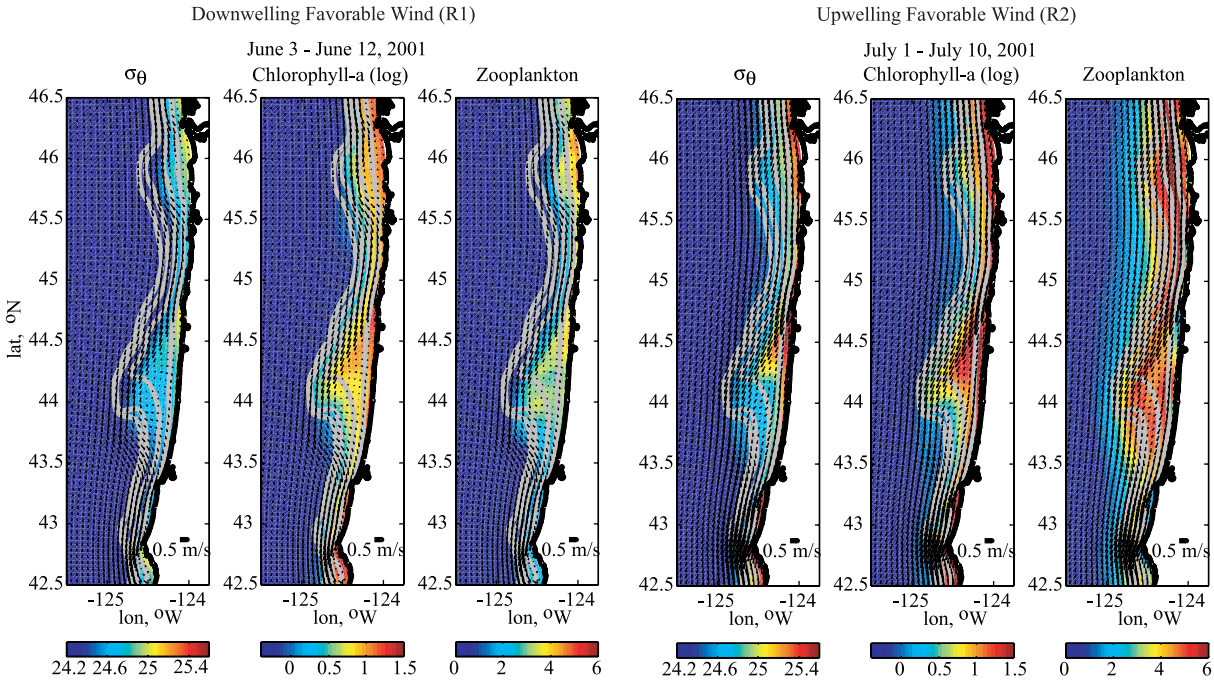

Figure 8. Time mean surface potential density σ_θ (kg m^{-3}), chlorophyll-*a* (mg Chl m^{-3}), and zooplankton (mmol N m^{-3}) for a period of (left) downwelling-favorable wind R1 and of (right) upwelling-favorable wind R2 during summer 2001. The arrows represent the mean surface velocity vectors for R1 and R2. The chlorophyll-*a* is plotted on a logarithmic (log 10) scale.

the bank. From the time series of the various concentrations (Figure 6), it is also clear that there is a strong relationship between the time-dependent wind forcing and the ecosystem response. Note in particular from Figure 7 the strong decreases in phytoplankton at Newport and at Heceta Bank during R1 and, in contrast, the sharp increases during R2. To study further the different responses of the ecosystem to these temporal changes in the wind stress and shelf circulation, we analyze in more detail the behavior during the two 10 day periods, R1 and R2, described by *Gan and Allen* [2005].

5.1. Periods of Upwelling and Downwelling

[23] While high surface chlorophyll-*a* and zooplankton are found on the shelf during summer 2001, the location of high zooplankton with respect to chlorophyll-*a* (Figure 8) varies considerably between periods of relaxation associated with mean downwelling-favorable wind (e.g., 3–12 June, R1) and periods of upwelling (e.g., 1–10 July, R2). During the downwelling-favorable period (R1), concentrations of zooplankton and chlorophyll-*a* are the highest inshore of the 50 m isobath, except on Heceta Bank where an offshore tongue of higher concentrations reaches the 100 m isobath. The highest zooplankton concentrations are noticeable in two regions (44.5°N and around 46°N) along the coast where the southward jet is weak, allowing increase of zooplankton biomass. The cyclonic circulation over and south of the bank induces a patch of higher zooplankton and chlorophyll-*a* concentration on the bank. During upwelling R2, the chlorophyll-*a* concentration is the highest inshore of the 100 m isobath where the surface potential density is high, reflecting the upwelling of water from depths where high concentrations of nutrient are present. High surface zooplankton concentration is found offshore of the 50 m isobath and offshore of the maximum phytoplankton. Zooplankton concentrations are largest in the coastal jet and in the secondary jet found next to the coast over the bank. Relatively high zooplankton concentrations are found offshore of the 200 m isobath south of Heceta Bank in a region of relatively weak surface currents. This region of high zooplankton biomass has been noticed in the field measurements (W. Peterson, personal communication, 2003). Low zooplankton concentrations near the coast are associated with upwelled water of high potential density (>25.6 kg m^{-3}) that is rich in nutrients and poor in zooplankton. Given the slower rate of zooplankton growth compared to phytoplankton, a small region (a few kilometers) next to the coast is left with almost no zooplankton but significant phytoplankton concentrations.

[24] Mean vertical sections at three locations during R1 (Figure 9) show clearly that the largest values of phytoplankton and of zooplankton concentrations are onshore of the coastal jet. The offshore scales of the high zooplankton concentrations are similar to those of high phytoplankton concentrations at Cascade Head and Newport, while relatively high zooplankton concentrations compared to phytoplankton concentrations are found farther offshore at Heceta Bank. This spatial distribution is, however, different during upwelling R2 (Figure 10). High zooplankton concentrations during R2 are considerably farther offshore than the high phytoplankton concentrations at the three sections. High zooplankton biomass is also located offshore of the coastal jet at the two northern sections, but remains onshore of the jet at Heceta Bank. A region of small zooplankton concen-

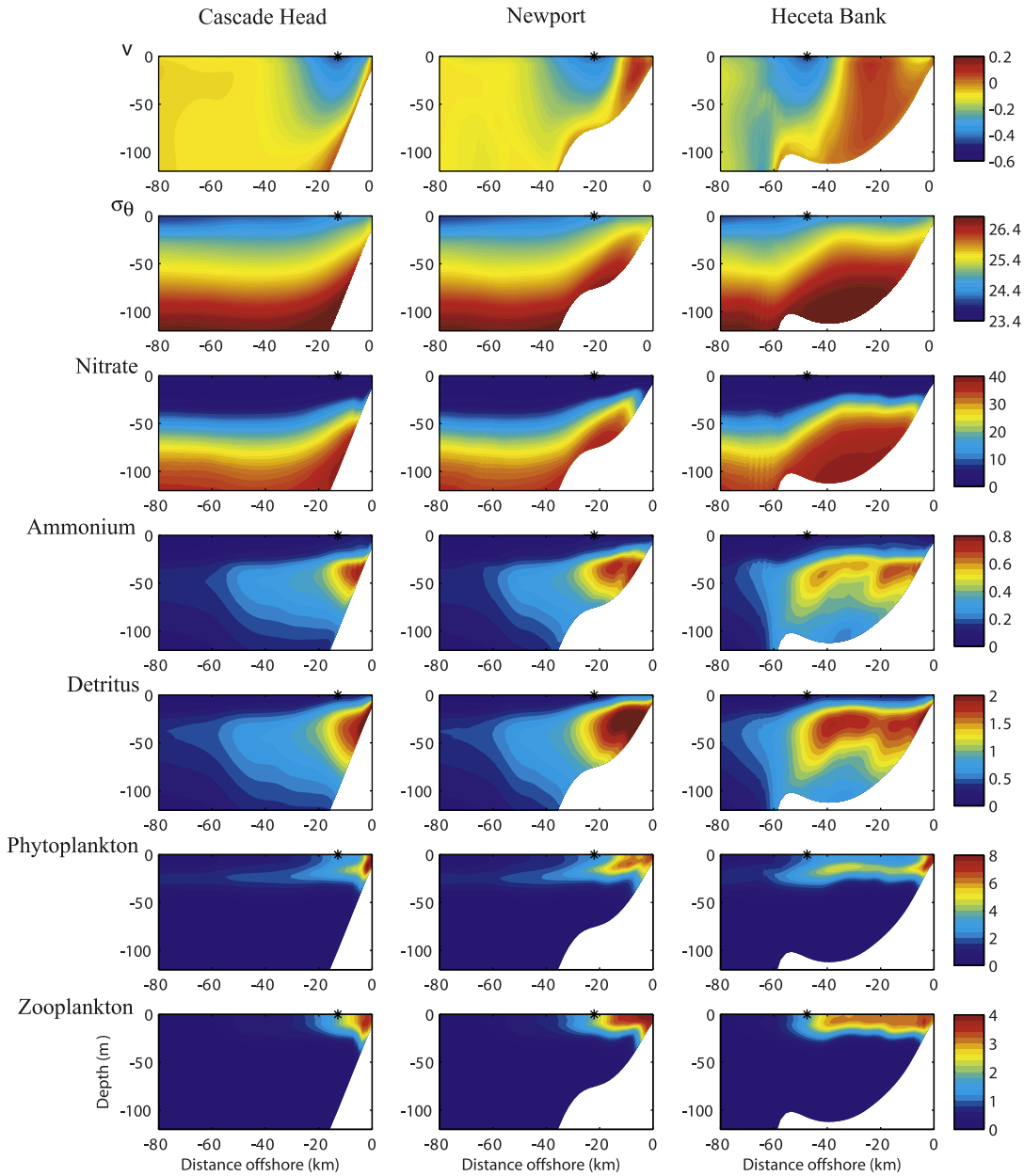

Figure 9. Time mean of the alongshore velocity v (m s^{-1}), the potential density σ_θ (kg m^{-3}), and the five components of the ecosystem model (mmol N m^{-3}) from 3 to 12 June 2001 (R1) at three sections (Cascade Head (200), Newport (175), and Heceta Bank (148)). The star corresponds to the position of the core of the coastal jet.

tration is visible close to shore at the three sections. Similar offshore distributions of phytoplankton and zooplankton were observed in a two-dimensional simulation [*Spitz et al.*, 2003] of the summer 1973, which was dominated by upwelling-favorable wind. On the bank, higher phytoplankton concentrations are found at the surface during R2 than R1. However, the deep chlorophyll-*a* maximum is more sharply defined during R1 than R2, which is due to stronger wind-induced mixing in the surface layer during R2 than R1. Zooplankton concentrations extend offshore to the core of the coastal jet over the bank during R1 and R2 with higher values during the R2 upwelling period. High zooplankton concentrations are found at greater depths during R2, due to stronger wind-induced surface mixing during that time period.

[25] The surface layer is depleted in nutrients (nitrate and ammonium) during the period R1. An accumulation of ammonium and detritus can be seen at depth below the layer of high zooplankton biomass. During R2, nutrients and detritus are upwelled near the coast, but since phytoplankton are taking up the nutrients inshore of the jet, there is no increase of nutrients at the surface. There is, however, a small region at the surface 20–40 km offshore associated with high zooplankton and low phytoplankton concentrations where ammonium reaches a value of about 0.2 mmol N m^{-3}. Higher concentrations of ammonium and detritus

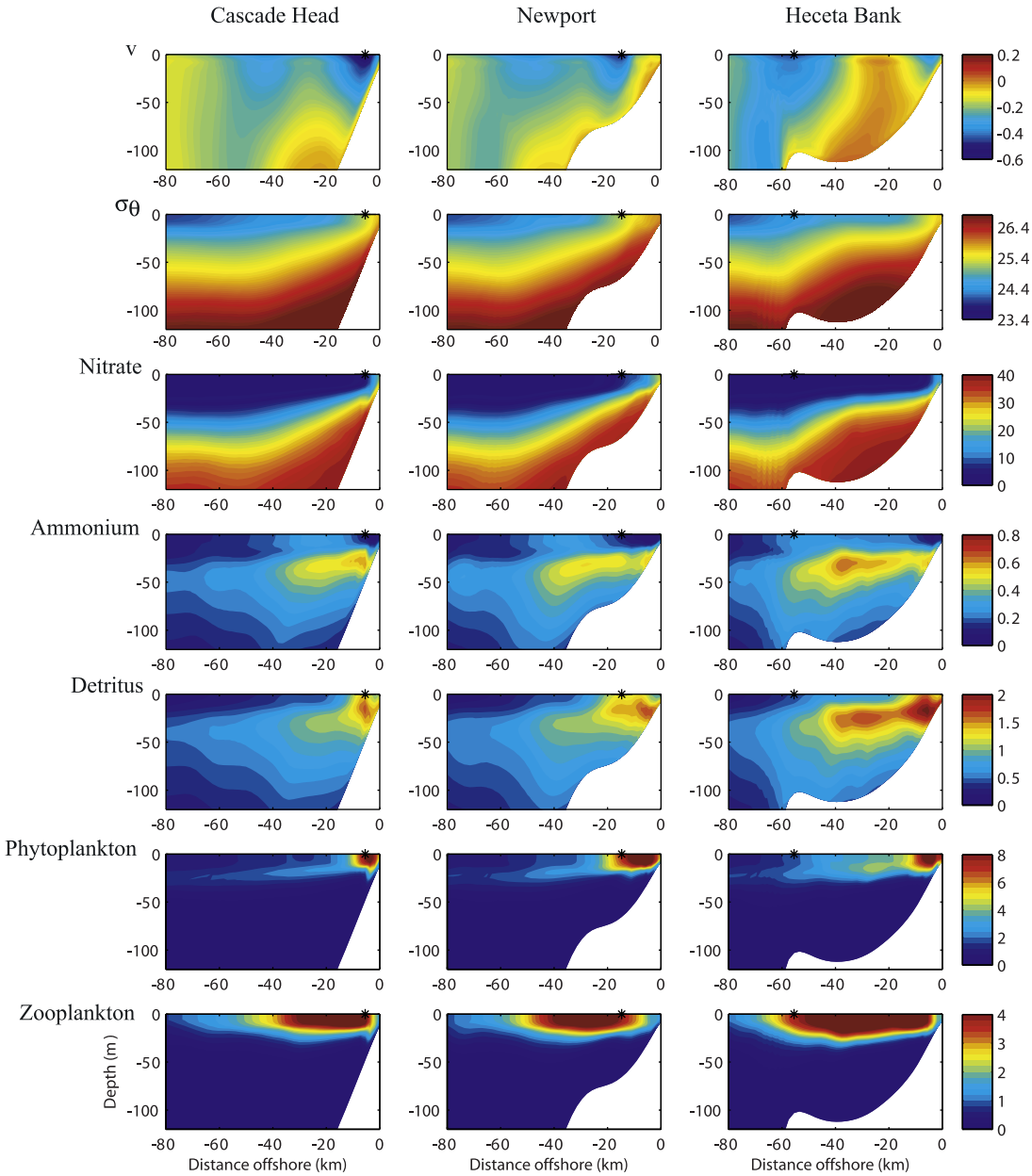

Figure 10. Time mean of the alongshore velocity v (m s^{-1}), the potential density σ_θ (kg m^{-3}), and the five components of the ecosystem model (mmol N m^{-3}) from 1 to 10 July 2001 (R2) at three sections (Cascade Head (200), Newport (175), and Heceta Bank (148)). The star corresponds to the position of the core of the coastal jet.

generally extend farther offshore during R2 than R1 due to larger offshore transport in the coastal jet at depth.

5.2. Term Balances During Upwelling and Downwelling

[26] We might expect that the relative importance of physical and biological forcing on the phytoplankton and zooplankton concentrations will vary both spatially and temporally between periods of upwelling and downwelling. To characterize this aspect of the ecosystem response, we evaluate and compare the physical forcing, corresponding to the sum of advection and diffusion, and the biological forcing, corresponding to the sum of source and sink terms in the ecosystem equations (1)–(5), for the periods of downwelling R1 and upwelling R2 (Figures 11–14).

[27] From the beginning to the end of the downwelling-favorable period R1 (Figure 11), the accumulation and removal of plankton along the coast is quite variable, resulting from the balance between physical and biological forcing. A decrease of phytoplankton occurs on the shelf and is the strongest onshore of the 50 m isobath and to about the 100 m isobath over Heceta bank (offshore tongue from 44.2°N to 44.5°N). A slight increase of surface zooplankton occurs inshore of the coastal jet while a slight

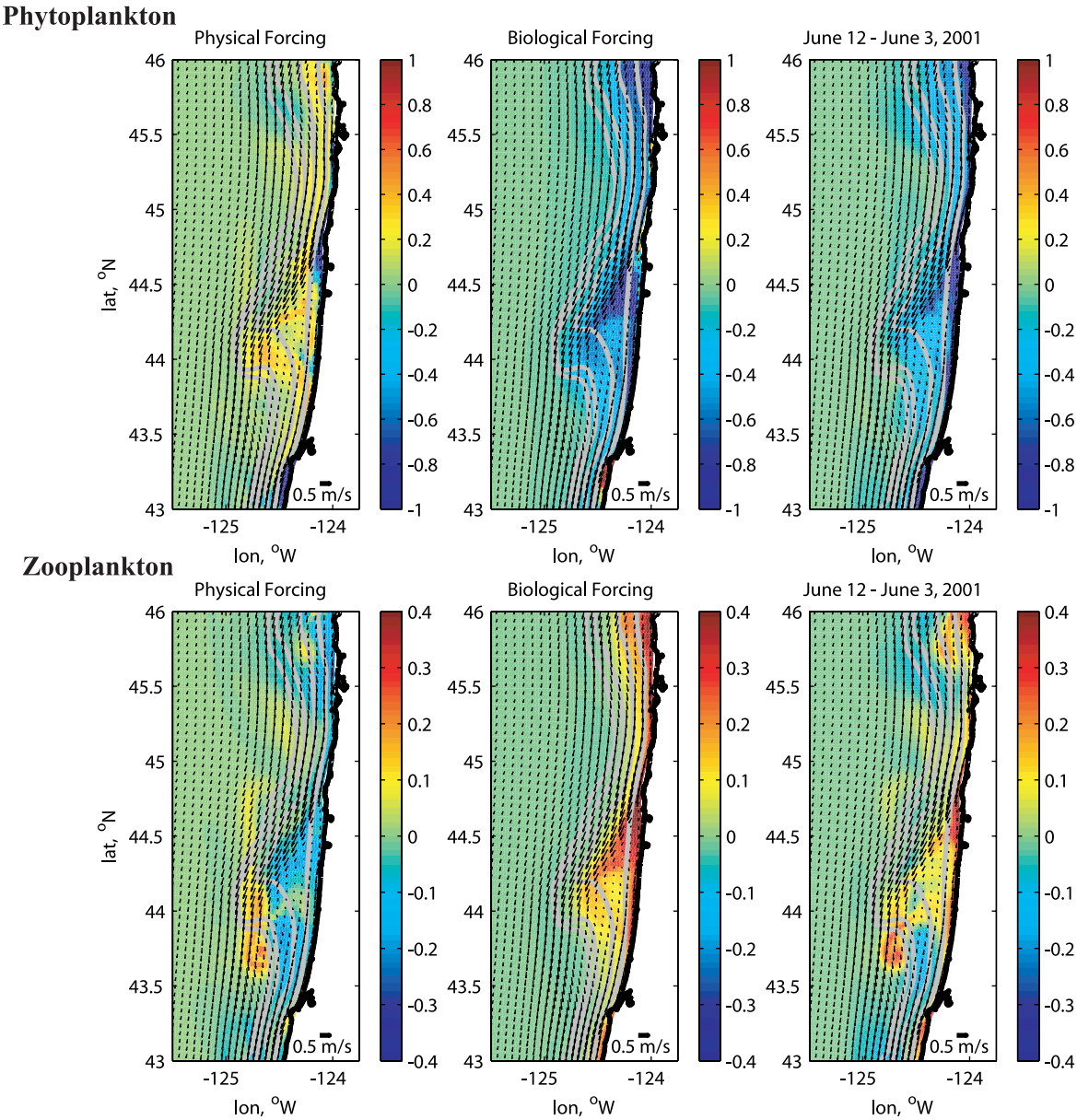

Figure 11. Time-averaged surface physical and biological balance (mmol N m^{-3} d^{-1}) for the phytoplankton and zooplankton over the downwelling period R1. The biological forcing is the sum of the ecosystem source and sink terms, and the physical forcing is the sum of the advection and diffusion terms. All the terms, except the time rate of change, are considered as on the right-hand side of the phytoplankton and zooplankton equations. As a result, the integrated time difference term equals the sum of the biological and physical forcing.

decrease is noticed offshore of the jet. The phytoplankton removal along the coast is due to a sink in the biological forcing that is larger than addition by physical forcing. Indeed, physical forcing (horizontal and vertical advection and diffusion) tends to accumulate phytoplankton slightly onshore of the coastal jet and more so on the bank. The phytoplankton biological sink is the result of strong zooplankton grazing pressure (Figure 12) that outcompetes the growth of phytoplankton due to the lack of nutrients at the surface. Strong grazing results in a source for the zooplankton during downwelling R1. The physical forcing, however, opposite to its effect on the phytoplankton, generally acts to remove zooplankton, except south of Heceta Bank where mesoscale features retain zooplankton. Excretion by zooplankton (Figure 12) seems to produce the surface ammonium that is taken up by phytoplankton. Zooplankton mortality is the largest in two nearshore regions that correspond to regions of higher grazing and larger phytoplankton growth.

[28] From the beginning to the end of the upwelling period R2 (Figure 13), phytoplankton increases slightly on the shelf inshore of the coastal jet while the largest increases occur on the bank. In contrast, zooplankton is removed from the same region by physical processes that overwhelm the

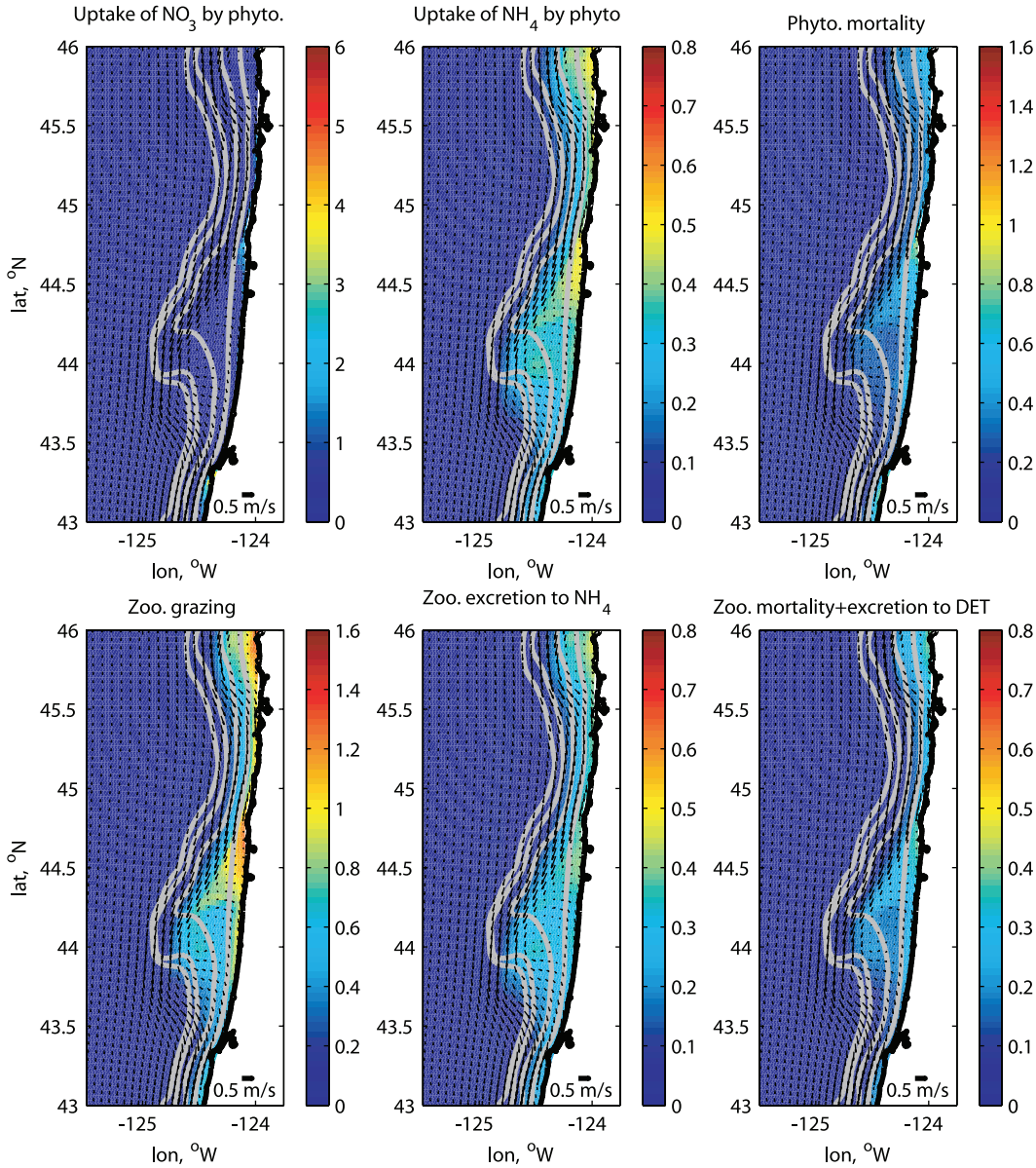

Figure 12. Time-averaged surface phytoplankton and zooplankton terms (mmol N m^{-3} d^{-1}) for the regime dominated by downwelling (R1). The arrows represent the mean surface velocity over the considered period. All terms are plotted as absolute values. Note the difference in the scales.

increase from the biological forcing. Physical processes, however, lead to an increase of zooplankton concentrations in regions offshore of the coastal jet. It is, indeed, interesting to note from the physical forcing that offshore mesoscale features seem to accumulate zooplankton off the shelf and to form patches with alongshore scales of about 40–50 km. For both variables, the physical forcing acts as a strong sink inshore of the 50 m isobath where upwelling of water poor in phytoplankton and zooplankton occurs. Decreases in the phytoplankton and zooplankton due to physical forcing also occur on the bank near 44.5°N and close to the 100 m isobath as a result of the offshore advection of the upwelled water. This upwelled and advected water is rich in nitrate, which results in high uptake by phytoplankton of nitrate and, to some extent, of ammonium (Figure 14). Because of the high nutrient availability, the nearshore phytoplankton growth is high and outcompetes grazing. The wedge-shaped region of relatively high biological forcing for the phytoplankton (Figures 13 and 14) that extends offshore over the shelf 20–30 km around 44.5°N reflects the increased upwelling of high-density water to the surface in the same general area (Figure 8). As shown by *Gan and Allen* [2005, Figure 19], in that location, on the inshore side of the coastal jet downstream of the separation point, alongshore advection of temperature, in addition to across shore advection, provides a significant contribution to the net cooling of the water column during R2. The net effect of combined alongshore and across shore advection presumably leads to the intensified upwelling, and hence to the greater productivity, in that region. Farther offshore,

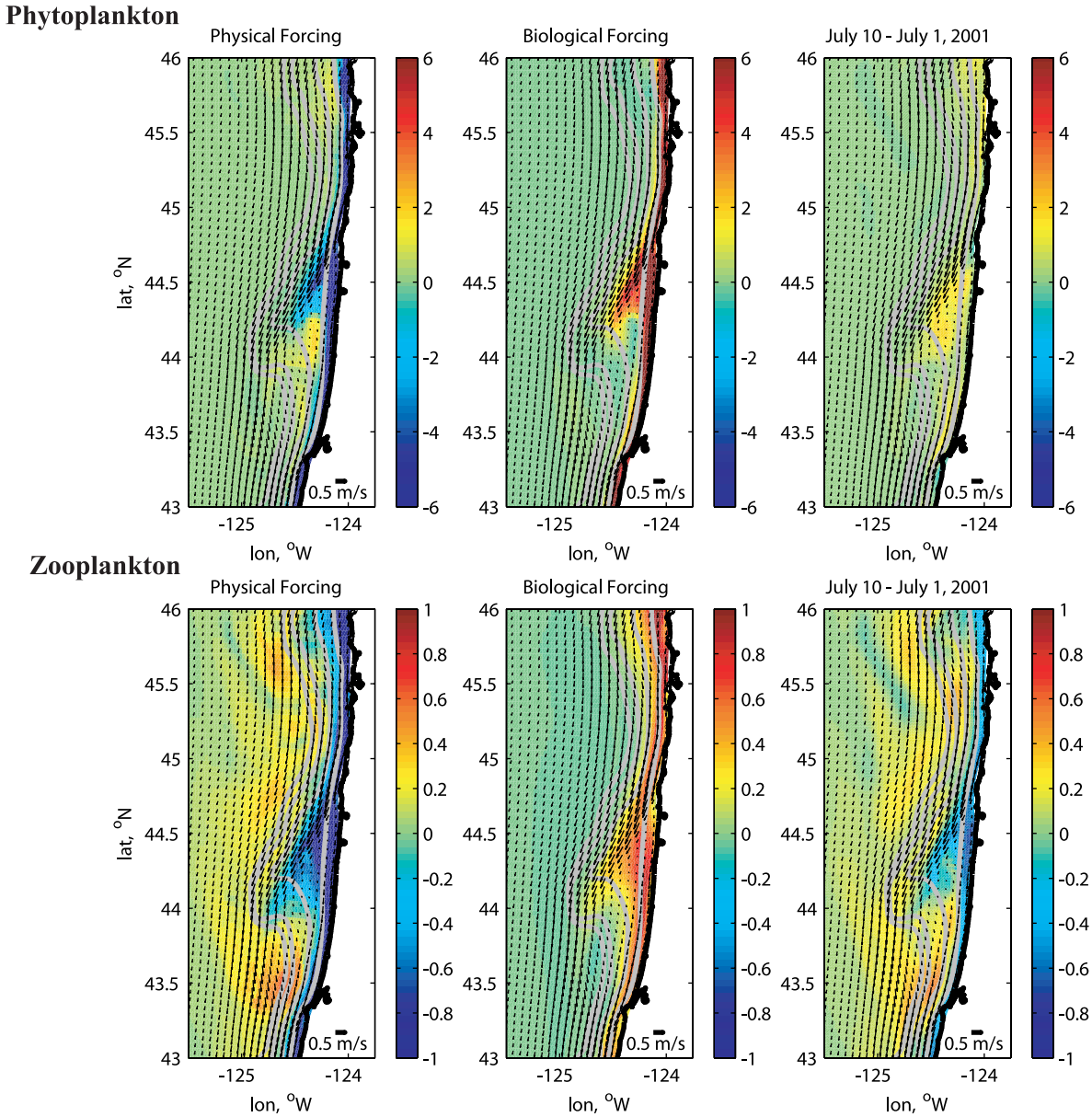

Figure 13. Same as Figure 11, but for the upwelling period R2.

smaller uptake of ammonium by phytoplankton is balanced by grazing, which limits growth of phytoplankton offshore of the 50 m isobath. The offshore pool of ammonium is evidently due to zooplankton excretion. Zooplankton mortality is the largest nearshore.

[29] Further information concerning the balance between physical and biological forcing can be obtained from analysis of the vertical structure of the forcing at the three sections with different topography. During downwelling R1 (Figure 15), the physical forcing removes phytoplankton from a very narrow region near the coast, but leads to an increase of surface phytoplankton on the inside of the jet and nearshore on the bottom. The strongest physical source is located near the jet at Heceta Bank. At the three sections, the region of negative physical forcing near the deep chlorophyll-*a* maximum (~30 m deep) results from a vertical displacement of that maximum. In the same region, there is a biological source of phytoplankton due to uptake of nitrate (not shown), which is clearly evident on Heceta Bank. At the three sections, the biological forcing acts as a removal of phytoplankton at the surface. The phytoplankton take up ammonium, but grazing of phytoplankton by zooplankton outcompetes the small growth due to low nutrient values at the surface. The decrease of phytoplankton due to lack of nutrients at the surface seems to extend slightly offshore to the coastal jet at Cascade Head. The balance between physical and biological forcing leads to a sink of phytoplankton in the surface layer and a slight increase around 30 m deep, especially on Heceta Bank. Physical forcing removes zooplankton from the surface, except near the jet on Heceta Bank. Surface zooplankton, via grazing of phytoplankton, grow at a relatively high rate near the coast and also on Heceta Bank at about 30 m depth in a region extending offshore about 50 km to the core of

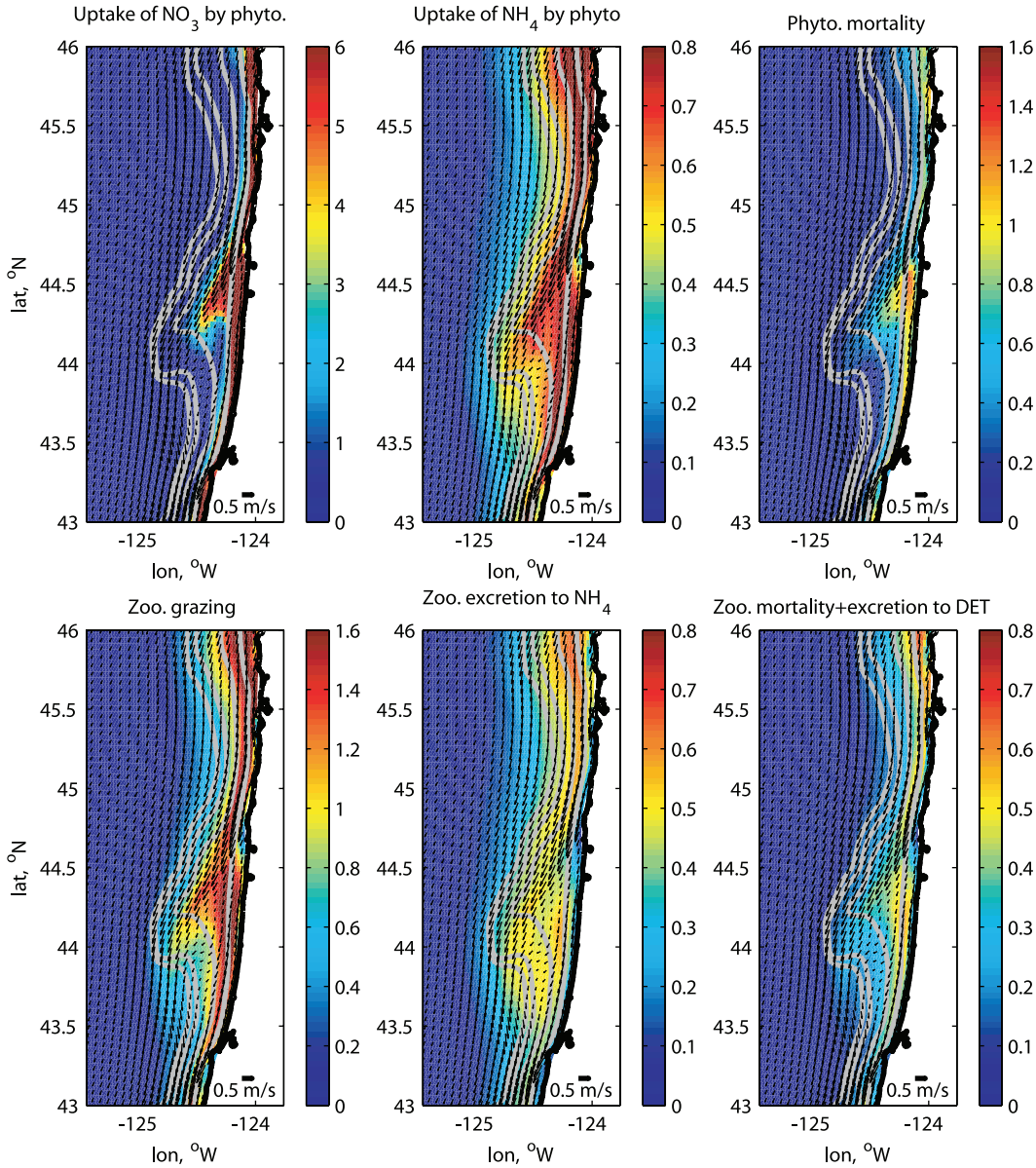

Figure 14. Same as Figure 12, but for the upwelling period R2. Note the difference in the scales.

the jet. This growth is larger than the loss due to the physics, thus resulting in an increase of zooplankton between the beginning and the end of the downwelling period.

[30] During the upwelling period R2 (Figure 16), physical forcing acts to remove phytoplankton at the surface from the coast to about 10 km offshore at Cascade Head and Heceta Bank. That removal extends farther offshore to about 20 km at Newport. The physical circulation on Heceta Bank leads to a considerable increase of phytoplankton in a region between 20 and 40 km offshore that extends to about 30 m deep. A small phytoplankton increase due to the physics is visible to about 15 m deep at Cascade Head and Newport, resulting from offshore transport of phytoplankton during upwelling. The biological forcing, through large uptake of nitrate inshore of the jet and smaller grazing by zooplankton (not shown), results in an increase of phytoplankton near the coast at the three sections. Grazing to about 20 m deep is the strongest between 5 and 20 km offshore. In addition, moderate grazing occurs to about 20 m deep and from 20 to 40 km offshore on Heceta Bank. Uptake of ammonium extends farther offshore than the uptake of nitrate at the three sections, with the source of ammonium being mainly from zooplankton excretion. Because of grazing, zooplankton biomass increases inshore of the jet. Physical forcing, however, removes zooplankton from these regions and accumulates zooplankton offshore of the jet. As a result of combined physical and biological forcing during upwelling, phytoplankton increase inshore of the coastal jet and zooplankton increase farther offshore. At Cascade Head and Newport, the zooplankton increase is offshore of the jet core, while at Heceta Bank the large increases are inshore of the jet.

[31] Primary productivity over the shelf at three sections along the Oregon coast (Figure 17) is mainly new productivity during upwelling (R2) as well as downwelling (R1). The *f* ratio (calculated for the model in a manner similar to

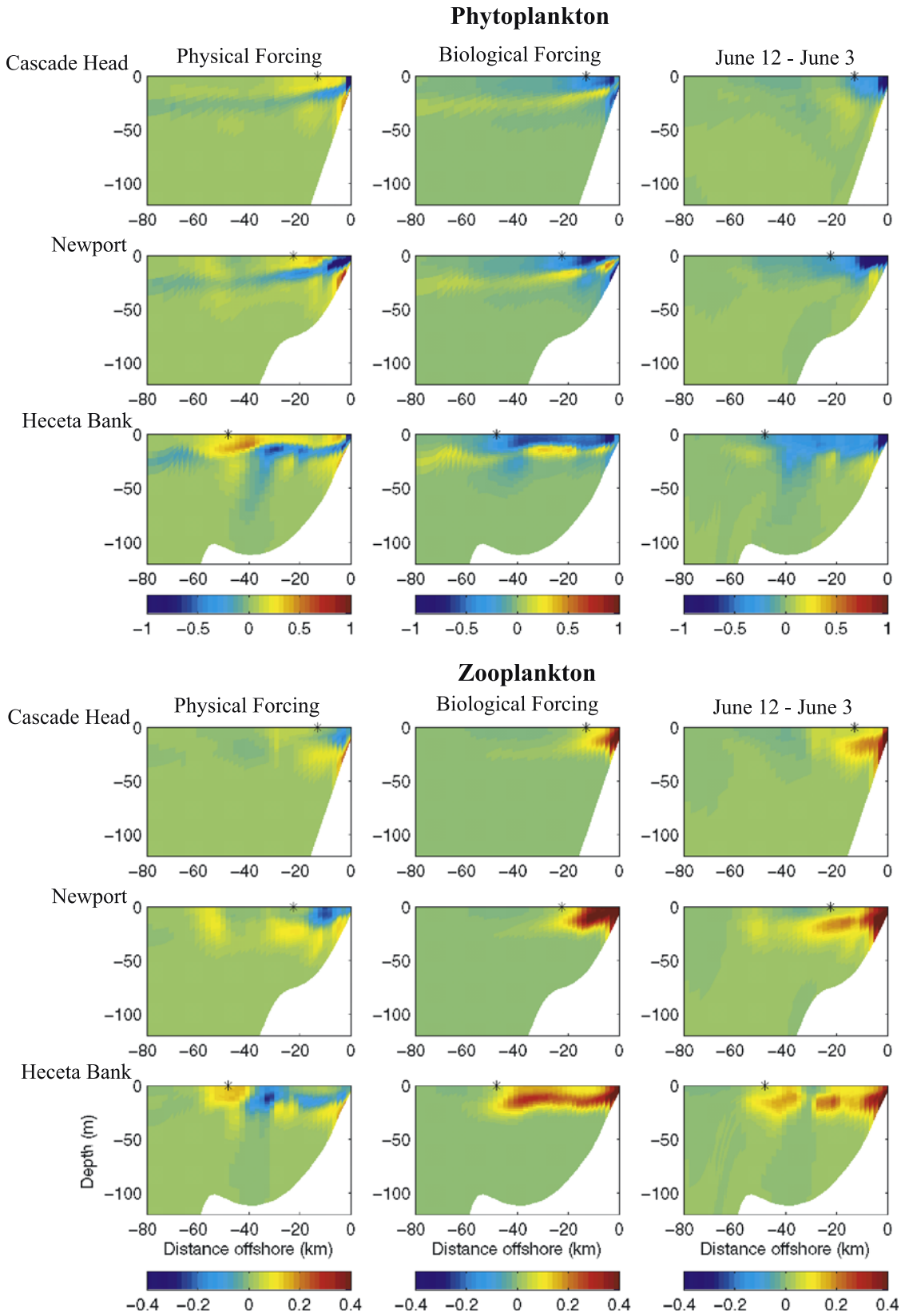

Figure 15. Time-averaged physical and biological balance (mmol N m^{-3} d^{-1}) for the phytoplankton and zooplankton over the downwelling period R1 and at three stations (Cascade Head (200), Newport (175), Heceta Bank (148)). The balance terms are defined the same as in Figure 11. The star corresponds to the position of the core of the coastal jet.

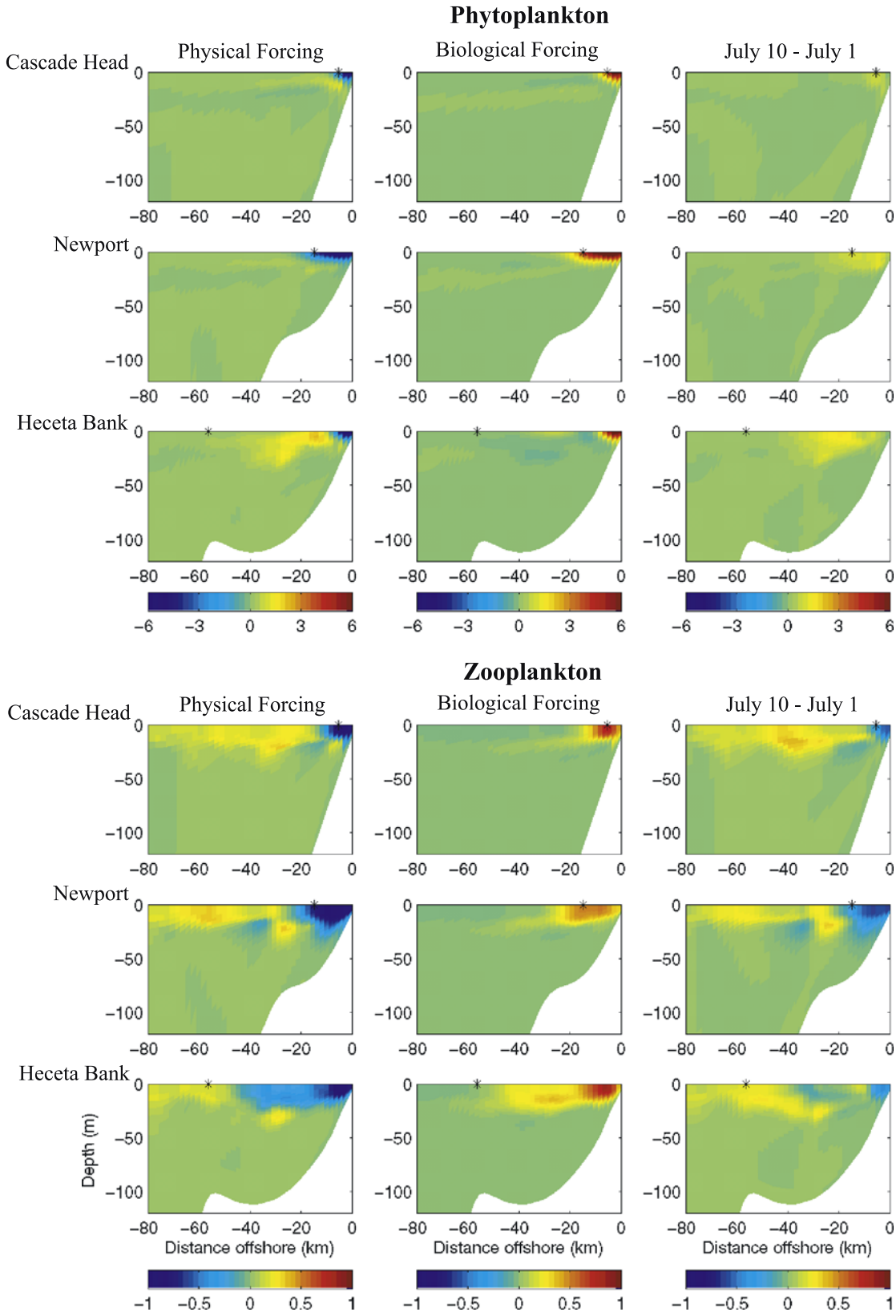

Figure 16. Same as Figure 15, but for the upwelling period R2.

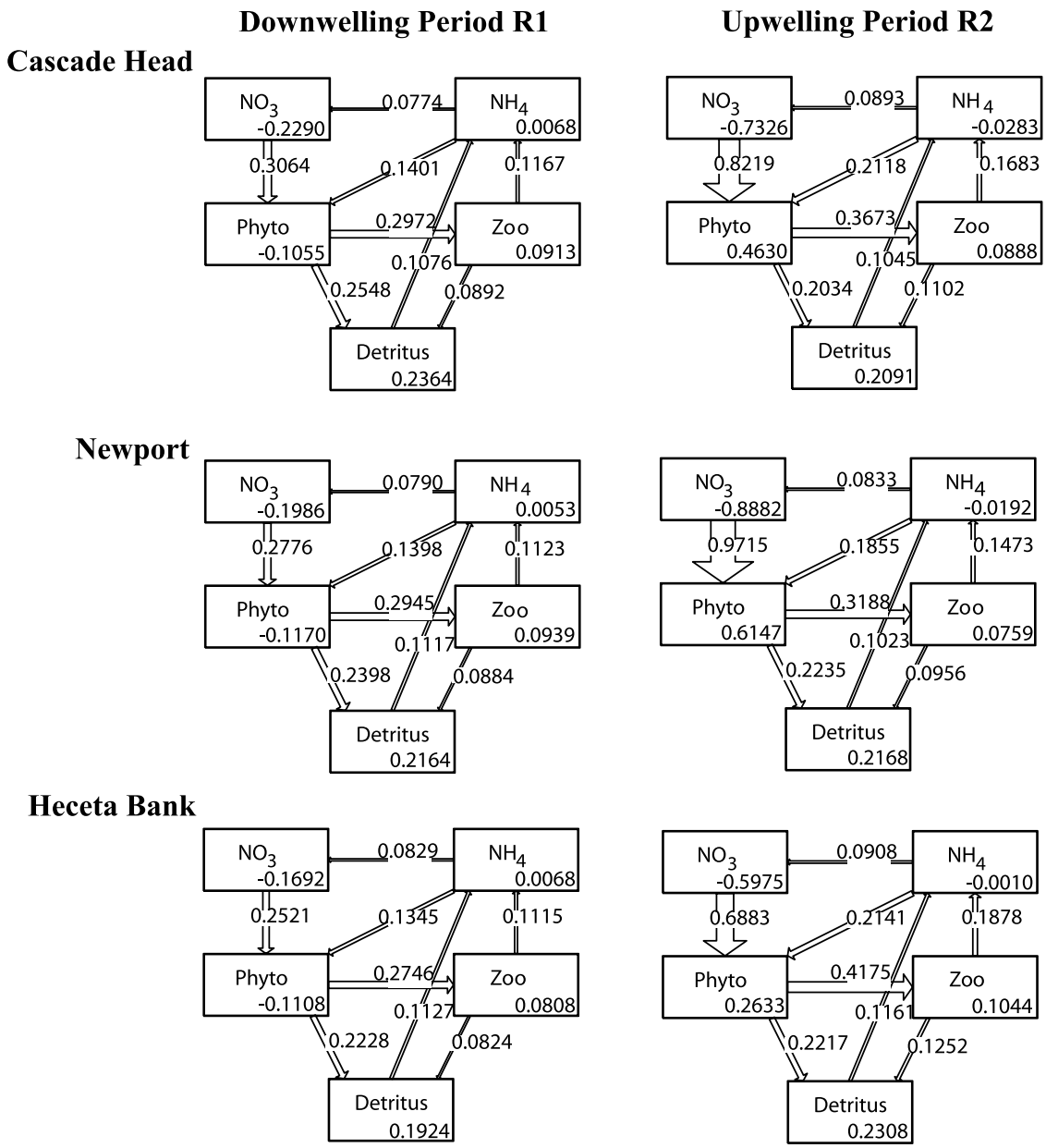

Figure 17. Fluxes (mmol N m^{-3} d^{-1}) due to biological sources and sinks during the downwelling R1 and upwelling R2 periods (averaged over the upper ocean coastal (UOC) region, i.e., from the surface to 60 m (or the bottom) and from the coast to the 200 m isobath). The numbers in the boxes are the average changes per day due to biological sources and sinks.

the observations, as specified by *Spitz et al.* [2003, equation (A20)]), however, is smaller on average during downwelling (0.67, 0.65, 0.66) than during upwelling (0.72, 0.82, 0.75) at the three sections (CH, NP, HB). On the other hand, the time evolution of the spatially averaged *f* ratio (Figure 7) shows a substantial range of variation during these periods, generally consistent with previous observations [*Dickson*, 1994]. During R1, it decreases from 0.67 to 0.4 while during R2, it increases from 0.69 to 0.88. Uptake of nitrate is the largest at Cascade Head for the period R1 and at Newport for the periods R2. During downwelling, uptake of ammonium is the largest at Cascade Head while, during upwelling, it is the largest at Heceta Bank. Grazing by zooplankton is larger during upwelling than downwelling at all three stations. While grazing during upwelling is the largest at Heceta Bank, during downwelling, it is the largest at Cascade Head. During upwelling, the biological forcing leads to an increase of phytoplankton, zooplankton and detritus at the three sections with a larger increase of phytoplankton at Newport. The zooplankton and detritus increases are the largest at Heceta Bank. Nitrate and ammonium decrease at the three sections with the largest nitrate decrease at Newport. During downwelling (R1), zooplankton, detritus and ammonium increase at the three sections due to biological forcing. The increase in zooplankton is the largest at Newport, while the detritus increase is the largest at Cascade Head. The phytoplankton and nitrate generally decrease during downwelling with the

Table 2. Net Changes of the Ecosystem Variables Integrated Over the UOC Region (Figure 7) During R1 and R2 Due to Biological Forcing and Due to the Combined Effect of Both Biological and Physical Forcing

	Cascade Head		Newport		Heceta Bank	
	Biology + Physics	Biology	Biology + Physics	Biology	Biology + Physics	Biology
			Downwelling (R1)			
NO_3	−0.1772	−0.2290	−0.2063	−0.1986	0.0388	−0.1692
NH_4	0.0117	0.0068	0.0096	0.0053	0.0086	0.0068
DET	−0.0271	0.2364	−0.0424	0.2164	−0.0317	0.1924
PHYTO	−0.1451	−0.1055	−0.1595	−0.1170	−0.1404	−0.1108
ZOO	0.1146	0.0913	0.1017	0.0939	0.0725	0.0808
			Upwelling (R2)			
NO_3	0.3277	−0.7326	0.5984	−0.8882	0.1840	−0.5975
NH_4	−0.0058	−0.0283	−0.0113	−0.0192	0.0011	−0.0010
DET	0.0082	0.2091	0.0038	0.2168	0.0558	0.2308
PHYTO	0.0331	0.4630	0.1309	0.6147	0.1723	0.2633
ZOO	−0.0482	0.0888	−0.0967	0.0759	0.0007	0.1044

largest decline at Cascade Head for the nitrate and at Newport for the phytoplankton. The changes due to the biological forcing during R1 and R2 (Figure 17) are compared in Table 2 to the net changes due the combined effect of the biological and physical forcing. The latter quantify the variations shown by the previously discussed time series in Figure 7. The differences in the fluxes and the average changes of the various concentrations between the three sections during upwelling and downwelling indicate again the complex interactions of the ecosystem and the physical circulation resulting from the alongshore variation in the shelf bottom topography associated with Heceta Bank.

6. Summary

[32] A nitrogen-based five component ecosystem model has been coupled to a high-resolution three-dimensional circulation model to study the response of the ecosystem to upwelling during the COAST field experiment in summer 2001. On the basis of field measurements and SeaWiFS images, the coupled circulation/ecosystem model reproduces the main spatial patterns and temporal behavior of the ecosystem variables observed along the Oregon coast.

[33] Simulation of the ecosystem response to upwelling off the Oregon coast shows features that reflect strong effects of the bottom topography in addition to the effects of time-variable winds. On average over the summer 2001, the winds are southward and upwelling-favorable, which leads to the development of a southward coastal jet and cold and nutrient rich water upwelled over the shelf. Relatively high mean values of chlorophyll-*a* are found in the surface layer onshore of the 50 m isobath, except over Heceta Bank where the coastal jet veers offshore, leading to an offshore spread of chlorophyll-*a* over the bank. Over the same period, relatively high mean zooplankton concentrations are found in the surface layer offshore of the coastal jet and offshore of the local maximum in mean chlorophyll-*a*, except on Heceta Bank where they extend out over the bank, but remain inshore of the coastal jet. This spatial distribution, however, is altered during periods of downwelling. During these periods, the largest mean zooplankton concentrations are found closer to shore and inshore of the coastal jet.

[34] An analysis of the balances between physical and biological forcing shows clearly the effect of the wind variability and of the topographical features on time evolution of the phytoplankton and zooplankton. During downwelling, grazing of phytoplankton by zooplankton is larger than addition of phytoplankton by physical forcing. Phytoplankton decreases along the coast. Physical forcing during downwelling generally acts to remove zooplankton, except south of Heceta Bank where mesoscale features retain zooplankton. As a result, a slight increase of surface zooplankton occurs inshore of the coastal jet while a slight decrease is found offshore of the jet. During upwelling, phytoplankton increases on the shelf inshore of the coastal jet while zooplankton increases in regions farther offshore. The increase of phytoplankton is the highest over Heceta Bank. For both variables, the physical forcing acts as a strong sink inshore of the 50m isobath, where upwelling of water poor in phytoplankton and zooplankton occurs. Because of the high nutrient availability, however, the nearshore phytoplankton growth is high, outcompeting grazing, and is larger than the physical sink.

[35] The model simulations show that the ecosystem response contains 20 day oscillations, similar to the oscillations present in the wind forcing. Increasing time lags are found between wind stress and nitrate (about 3 days), wind stress and phytoplankton (about 7 days) and wind stress and zooplankton (13–16 days). Phytoplankton decorrelation timescales are approximately 6–8 days over the shelf and are comparable to the decorrelation timescales of 10 days for larger spatial scales found from satellite observations [*Denman and Abbott*, 1988, 1994].

[36] **Acknowledgments.** The research was supported by the National Science Foundation Coastal Ocean Progresses (CoOP) program under grant OCE-9907854. The authors wish to thank their coinvestigators from the COAST program for providing data for comparison with the model output and for numerous helpful discussions. The authors also thank two anonymous reviewers for their helpful comments.

References

Austin, J. A., and J. A. Barth (2002), Variation in the position of the upwelling front on the Oregon shelf, *J. Geophys. Res.*, *107*(C11), 3180, doi:10.1029/2001JC000858.

Bane, J. M., M. D. Levine, R. M. Samelson, S. M. Haines, M. F. Meaux, N. Perlin, P. M. Kosro, and T. Boyd (2005), Atmospheric forcing of the Oregon coastal ocean during the 2001 upwelling season, *J. Geophys. Res.*, doi:10.1029/2004JC002653, in press.

Barth, J. A., S. D. Pierce, and R. L. Smith (2000), A separating coastal upwelling jet at Cape Blanco, Oregon and its connection to the California

Current System, *Deep Sea Res., Part II*, *47*, 783–810, doi:10.1016/S0967-0645(99)00127-7.

Barth, J. A., R. O'Malley, and A. Y. Erofeev (2003), SeaSoar observations during the Coastal Ocean Advances in Shelf Transport (COAST) Survey I: 23 May–13 June 2001, *Data Rep. 191, Ref. 03-1*, Coll. of Oceanic and Atmos. Sci., Oreg. State Univ., Corvallis.

Barth, J. A., S. D. Pierce, and R. M. Castelao (2005), Time-dependent, wind-driven flow over a shallow midshelf submarine bank, *J. Geophys. Res.*, doi:10.1029/2004JC002761, in press.

Blumberg, A. F., and G. L. Mellor (1987), A description of a three dimensional coastal ocean circulation model, in *Three Dimensional Coastal Ocean Models*, *Coastal and Estuarine Sci. Ser.*, vol. 4, edited by N. Heaps, pp. 1–16, AGU, Washington, D. C.

Bosch, J. A., A. C. Thomas, and P. T. Strub (2002), Satellite-measured chlorophyll variability within the upwelling zone near Heceta Bank, Oregon, *Eos Trans. AGU*, *83*(4), Ocean Sci. Meet. Suppl., Abstract OS31D-57.

Castelao, R. M., and J. A. Barth (2005), Coastal ocean response to summer upwelling favorable winds in a region of alongshore bottom topography variations off Oregon, *J. Geophys. Res.*, *110*, C10S04, doi:10.1029/2004JC002409.

Chase, Z., B. Hales, T. J. Cowles, R. Schwartz, and A. van Geen (2005), Distribution and variability of iron input to Oregon coastal waters during the upwelling season, *J. Geophys. Res.*, *110*, C10S12, doi:10.1029/2004JC002590.

Corwith, H. L., and P. A. Wheeler (2002), El Niño related variations in nutrient and chlorophyll distributions off Oregon, *Prog. Oceanogr.*, *54*, 361–380.

Denman, K. L., and M. R. Abbott (1988), Time evolution of surface chlorophyll patterns from cross-spectrum analysis of satellite color images, *J. Geophys. Res.*, *93*, 6789–6798.

Denman, K. L., and M. R. Abbott (1994), Time scales of pattern evolution from cross-spectrum analysis of advanced very high resolution radiometer and coastal zone color scanner imagery, *J. Geophys. Res.*, *99*, 7433–7442.

Dickson, M.-L. (1994), Nitrogen dynamics in a coastal upwelling regime, Ph.D. dissertation, 227 pp., Oreg. State Univ., Corvallis.

Dickson, M.-L., and P. A. Wheeler (1995), Nitrate uptake rates in a coastal upwelling regime: A comparison of PN-specific, absolute, and Chl a-specific rates, *Limnol. Oceanogr.*, *40*, 533–543.

Dugdale, R. C., and F. P. Wilkerson (1989), New production in the upwelling center at Point Conception, California: Temporal and spatial patterns, *Deep Sea Res.*, *36*, 985–1007.

Edwards, C. A., H. P. Batchelder, and T. M. Powell (2000), Modeling microzooplankton and macrozooplankton dynamics within a coastal upwelling system, *J. Plankton Res.*, *22*, 1619–1648.

Gan, J. P., and J. S. Allen (2002), A modeling study of shelf circulation of northern California in the region of the Coastal Ocean Dynamics Experiment: 2. Simulation and comparison with observations, *J. Geophys. Res.*, *107*(C11), 3184, doi:10.1029/2001JC001190.

Gan, J., and J. S. Allen (2005), Modeling upwelling circulation off the Oregon coast, *J. Geophys. Res.*, *110*, C10S07, doi:10.1029/2004JC002692.

Gan, J., J. S. Allen, and R. M. Samelson (2005), On open boundary conditions for a limited-area coastal model off Oregon. part 2: Response to wind forcing from a regional mesoscale atmospheric model, *Ocean Modell.*, *8*, 155–173, doi:10.1016/j.ocemod.2003.12.007.

Huyer, A. (1983), Coastal upwelling in the California Current system, *Prog. Oceanogr.*, *12*, 259–284.

Karp-Boss, L., P. A. Wheeler, B. Hales, and P. Covert (2004), Distributions and variability of particulate organic matter in a coastal upwelling system, *J. Geophys. Res.*, *109*, C09010, doi:10.1029/2003JC002184.

Kokkinakis, S. A., and P. A. Wheeler (1988), Uptake of ammonium and urea in the northeast Pacific: Comparison between netplankton and nanoplankton, *Mar. Ecol. Prog. Ser.*, *43*, 113–124.

Kosro, P. M. (2005), On the spatial structure of coastal circulation off Newport, Oregon, during spring and summer 2001 in a region of varying shelf width, *J. Geophys. Res.*, doi:10.1029/2004JC002769, in press.

Lamb, J., and W. Peterson (2005), Ecological zonation of zooplankton in the COAST study region off central Oregon in June and August 2001 with consideration of retention mechanisms, *J. Geophys. Res.*, *110*, C10S15, doi:10.1029/2004JC002520.

Large, W. G., and S. Pond (1981), Open ocean momentum flux measurements in moderate to strong winds, *J. Phys. Oceanogr.*, *11*, 324–336.

Newberger, P. A., J. S. Allen, and Y. H. Spitz (2003), Analysis and comparison of three ecosystem models, *J. Geophys. Res.*, *108*(C3), 3061, doi:10.1029/2001JC001182.

Oke, P. R., J. S. Allen, R. N. Miller, G. D. Egbert, J. A. Austin, J. A. Barth, T. J. Boyd, P. M. Kosro, and M. D. Levine (2002), A modeling study of the three-dimensional continental shelf circulation off Oregon. part I: Model-data comparisons, *J. Phys. Oceanogr.*, *32*, 1360–1382.

O'Malley, R., J. A. Barth, and A. Y. Erofeev (2002), SeaSoar observations during the Coastal Ocean Advances in Shelf Transport (COAST) Survey II, W0108A, 6–25 August 2001, *Data Rep. 186, Ref. 02-2*, Coll. of Oceanic and Atmos. Sci., Oreg. State Univ., Corvallis.

Powell, T. M., G. V. W. Lewis, E. N. Curchitser, D. B. Haidvogel, A. J. Hermann, and E. L. Dobbins (2005), Results from a three-dimensional, nested biological-physical model of the California current system and comparisons with statistics from satellite imagery, *J. Geophys. Res.*, doi:10.1029/2004JC002506, in press.

Samelson, R., P. Barbour, J. Barth, S. Bielli, T. Boyd, D. Chelton, P. Kosro, M. Levine, and E. Skyllingstad (2002), Wind stress forcing of the Oregon coastal ocean during the 1999 upwelling season, *J. Geophys. Res.*, *107*(C5), 3034, doi:10.1029/2001JC000900.

Service, S. K., J. A. Rice, and F. P. Chavez (1998), Relationship between physical and biological variables during the upwelling period in Monterey Bay, CA, *Deep Sea Res., Part II*, *45*, 1669–1685.

Small, L. F., and D. W. Menzies (1981), Patterns of primary productivity and biomass in a coastal upwelling region, *Deep Sea Res., Part A*, *28*, 123–149.

Smith, R. L. (1974), A description of current, wind and sea level variations during coastal upwelling off the Oregon coast, July–August 1972, *J. Geophys. Res.*, *79*, 435–443.

Spitz, Y. H., P. A. Newberger, and J. S. Allen (2003), Ecosystem response to upwelling off the Oregon coast: Behavior of three nitrogen-based models, *J. Geophys. Res.*, *108*(C3), 3062, doi:10.1029/2001JC001181.

Wroblewski, J. S. (1977), A model of phytoplankton plume formation during variable Oregon upwelling, *J. Mar. Res.*, *35*, 357–394.

J. S. Allen and Y. H. Spitz, College of Oceanic and Atmospheric Sciences, Oregon State University, Corvallis, OR 97331, USA. (jallen@coas.oregonstate.edu; yvette@coas.oregonstate.edu)

J. Gan, Department of Mathematics and Atmospheric, Marine and Coastal Environment Program, Hong Kong University of Science and Technology, Kowloon, Hong Kong. (magan@ust.hk)